CALPHAD: Computer Coupling of Phase Diagrams and Thermochemistry 89 (2025) 102825

Contents lists available at ScienceDirect

Calphad

journal homepage: www.elsevier.com/locate/calphad

Multicomponent cluster variation method: Application to high entropy alloys

Vikas Jindal *, Shrikant Lele

Department of Metallurgical Engineering, IIT(BHU), Varanasi, 221005, India

ARTICLE INFO

Handling Editor: Prof. Z.K. Liu

Keywords:
Cluster expansion
Cluster variation method
CALPHAD

ABSTRACT

Cluster expansion, a method commonly used in computational thermodynamics, expresses the configurational properties of alloys as a sum of products of correlation functions and cluster expansion coefficients (CECs). The CECs are defined using a basis in configurational space that is not unique and changes during the extension of the generalized Ising model from binary alloys to multicomponent alloys. In contrast to the CALPHAD formulation, this change severely restricts the development and use of CEC-based databases. To address this, a new framework is introduced where lower-order CECs remain unchanged in higher-order systems. This is achieved by choosing configurational variables (and corresponding CECs) which are not dependent on a particular choice of basis as correlation functions (CFs). Such a set is provided by cluster variables (CVs), which represent the fraction of cluster configurations of various types. A carefully selected subset of independent CVs is chosen as CFs. Completeness of the basis is demonstrated by deriving expressions for all remaining CVs in terms of these new CFs for disordered bcc, fcc, and hcp structures. A set of CECs for the bcc phase of the Nb-Ti-V-Zr system has been developed using this new formulation. Optimized CECs of all binary and ternary subsystems of the Nb-Ti-V-Zr have been used in its construction. This is a crucial step towards creating a self-consistent computational thermodynamics database. The utility of the Nb-Ti-V-Zr database was demonstrated through calculations of thermodynamic quantities, SRO parameters, and phase diagrams. Additionally, a procedure is outlined to transform existing CALPHAD databases to CEC-based databases under certain assumptions.

1. Introduction

Cluster expansions of any configurational property have become common in the computational thermodynamics of alloys [1–24]. Most of the applications have been restricted to binary alloys. On the other hand, real alloys are invariably multicomponent alloys. The configurational state of an alloy is expressed in terms of independent configurational variables designated as correlation functions (CFs) corresponding to each crystallographically distinct cluster of atomic sites in a crystal. Any configurational property can then be expressed as a bilinear sum of the products of CFs and corresponding coefficients called cluster expansion coefficients (CECs) or effective cluster interactions (ECIs). The configuration space spanned by the CFs is usually specified in terms of a basis that is not unique [1,25–30]. Sanchez et al. [1] used an orthogonal basis based on Chebychev polynomials. A simple geometrical interpretation for this basis is given by Cenedese and Gratias [31]. Modified Chebychev polynomials were used by Sarma and Lele [27]. A variable basis was used by Sanchez and Mohri [32] in which the point CF becomes equal to '0' for the chosen composition. This is a generalization of the Chebychev polynomial basis. Taggart [25] suggested a spin variables-based basis set consisting of the successive powers of the pseudo-spin configuration variable $\{\sigma\}$. Later, Inden and Pitsch [26] developed another basis by a method that is equivalent to that of Taggart. These bases have an advantage over Chebychev polynomials in numerically intensive calculations because these functions are always integers. Wolverton and de Fontaine [33] have suggested the complex cubic roots of unity (exponential functions) as well as pair probabilities (considering only pair cluster interactions) as bases for ternary systems and have also compared various basis functions. Fernández-Caballero et al. [30] have used trigonometric basis functions (instead of complex exponential functions) similar to those used in the ATAT program [28]. The solvent and sublattice-solvent bases have been used for find limiting values of CFs for binary disordered and ordered phases, respectively, by Sarma [34] and Gorrey et al. [35]. This choice of basis makes the correlation functions identical to some of the cluster probabilities (those not involving one chosen component which acts as the solvent) and is

* Corresponding author.
E-mail address: vjindal.met@iitbhu.ac.in (V. Jindal).

https://doi.org/10.1016/j.calphad.2025.102825
Received 18 September 2024; Received in revised form 13 March 2025; Accepted 13 March 2025

numerically advantageous in calculations involving dilute alloys. A similar approach was proposed by Zhang and Sluiter [29]. None of these basis functions is symmetric or anti-symmetric with respect to the components.

Extension of the generalized Ising model for binary alloys to multicomponent alloys changes the dimensionality of the configuration space and, thus, of the basis. This, in turn, leads to changes in the CFs and CECs for the same subclusters in going from a (κ–1)-component system to a κ-component one. Sarma and Lele [27] discussed these issues and showed a scheme for transforming the CEC of a lower order system to a higher order system, which was necessary due to the basis change. Zhang and Sluiter [29] have argued that the CECs of a lower order subsystem in the solvent basis can be incorporated into the CECs of a higher order system without any transformation. This statement holds only so long as the higher order system contains the component treated as solvent for the subsystem but is not valid in general irrespective of the choice of basis set functions available in literature.

The object of this communication is to present a formalism for choosing CFs for disordered phases from among the cluster variables which ensures that CECs of subsystems can be directly inherited in the cluster expansion of a higher-order system. The choice is guided by the requirement that the CFs reduce, in the point approximation, to the Redlich-Kister polynomials [36] for binary alloys and to those used in CALPHAD formulations for multicomponent systems [37]. The fact that the set of CECs of all subsystems can be used in the cluster expansion of a higher-order system is of great advantage in the development of a self-consistent database of multicomponent CECs required for Computational Thermodynamics.

This paper is organized as follows. Details of the derivation of multicomponent cluster expansion based on cluster variables for the disordered bcc structure are given in section 2. Correlation functions and cluster variables for disordered fcc and hcp structures are given in Appendix 1 and 2, respectively. The thermodynamics of bcc phase in the Nb-Ti-V-Zr systems has been studied with a view to provide deeper understanding of the effects of entropy and enthalpy in the stabilization of this phase utilizing the new CE formulation. Section 3 provides details of the procedure for obtaining an optimized set of CECs for the bcc phase of the Nb-Ti-V-Zr system. Various thermodynamic calculations based on multicomponent cluster expansion of the Nb-Ti-V-Zr system are presented in Section 4. Short range order parameter calculations for the bcc phase at different compositions and temperatures are also presented in this section.

We note that the present formulation pertains only to the configurational contribution to alloy thermodynamics based on a rigid lattice. Generally, there are changes in the volume on alloying, which also lead to changes in the thermodynamic quantities [24]. Further, vibrational contributions also need to be considered for a more accurate description of alloy thermodynamics [38,39].

2. Multicomponent cluster expansion based on cluster variables

We will try to write a cluster expansion of the energy using a selected set of Cluster Variables (CVs) instead of the conventional Correlation Functions (CFs). The selection is based on the following criteria:

(i) The CVs or a simple combination of CVs selected to replace the conventional CFs should be capable of being used in higher-order systems without transformation, that is, they should be directly inherited.

(ii) The cluster configuration for a ν-point CV or combination of ν-point CVs representing a CF in a particular κ-component system should include all the components of the system if $\nu \geq \kappa$ and at least ν components if $\nu < \kappa$.

For $\nu \geq \kappa$, including all κ components ensures that the CF is symmetric and representative of the entire κ-component system. This prevents asymmetry in the CFs and the cluster expansion coefficients (CECs). For example, in a tetrahedron CV ($\nu = 4$) for a binary system ($\kappa = 2$), inclusion of only one component would introduce an asymmetry in the CVs, which would cascade into the CECs. This would affect the inheritance of lower-order CFs and CECs into those of higher-order systems and pose challenges when creating multicomponent databases.

For $\nu < \kappa$, the condition ensures that the CF remains relevant to the ν-component subsystem. For instance, in the case of a pair CV ($\nu = 2$) in a quaternary system ($\kappa = 4$), including at least two components allows the generation of all six possible types of pair CVs. Omitting this requirement, such as including only one component, would result in only four types of pair CVs, making it difficult to construct an independent and complete set of CVs.

(iii) It should be symmetric or anti-symmetric in the components present in the cluster configuration as far as possible. For $\nu \geq \kappa$, it should also be unique to that system and should not represent a CF in any other system of the same order. For $\nu < \kappa$, the CV or combination of CVs representing a CF is the same as for the corresponding ν -component system.

The requirement for correlation functions to be symmetric or antisymmetric in the components of the cluster configuration stems from the need to maintain consistency and completeness in the representation of the system's interactions. Symmetry is preferred wherever possible because it ensures that the correlation function treats all components in the cluster equivalently, avoiding preference for any specific component. However, for clusters with an odd number of points, it is mathematically impossible to achieve symmetry in the components. In such cases, the correlation functions are chosen to be antisymmetric to maintain internal consistency and adhere to well-defined conventions. The ambiguity regarding the sign in antisymmetric correlation functions is resolved by following a consistent convention. Specifically, the sign is determined based on the alphabetical ordering of the component names. This convention ensures reproducibility and eliminates subjectivity in determining the sign, making antisymmetric correlation functions just as valid as symmetric ones in representing the system.

We shall now explain the general formalism used to specify the configuration of an alloy and then illustrate this approach for the disordered *bcc* (A2), *fcc* (A1), and *hcp* (A3) phases.

2.1. Configurational variables

Consider a disordered crystalline system with N crystallographically equivalent atomic sites. The configuration of the κ-component alloy can be specified completely in terms of the type of atom (A, B …, Z) occupying each site. Towards this end, site occupation operators are defined as binary variables [40] through.

$p_i^P = 1$, if atom of type P occupies site i, $P \in \{A, B, \ldots Z\}$ which is an alphabetically ordered set of the names of the components and Z is the κ^{th} component.

$= 0$ otherwise

In case vacancies are to be considered, they can be treated as one of the components. We shall, therefore, not specifically mention vacancies separately. Since each site is occupied by only one atom

$$\sum_A^Z p_i^P = 1 \quad \text{for all } i \tag{1}$$

Thus, the configuration of the system can be completely prescribed by specifying any set of ($\kappa - 1$) site occupation operators for each of the N sites of the crystal. Alternately, an arbitrary set of ($\kappa - 1$) independent functions of the κ site occupation operators, called site operators, can be chosen to represent the configuration. The same set of site occupation operators or site operators need to be used for all crystallographically equivalent sites in a crystal [35].

A pair occupation operator p_{ij}^{PR} for an arbitrary pair cluster consisting

of sites, i and j can be defined as a binary variable that takes the value 1 if an atom of type P occupies site i and simultaneously an atom of type R occupies site j, otherwise, it takes the value 0. From the binary nature of these operators, it follows readily that

$$p_{ij}^{PR} = p_i^P \bullet p_j^R \quad P,R = A,B\ldots Z \text{ for all } i,j \tag{2}$$

and therefore

$$\begin{gathered}\sum_P \sum_R p_{ij}^{PR} = \sum_P \sum_R p_i^P \bullet p_j^R = \sum_P p_i^P \bullet \sum_R p_j^R = 1, \\ \sum_R p_{ij}^{PR} = \sum_R p_i^P \bullet p_j^R = p_i^P \bullet \sum_R p_j^R = p_i^P\end{gathered} \tag{3}$$

The above relations are known as normalization and geometric reduction constraints, respectively. Relations of the type of Eqns. (2) and (3) among the pair occupation operators imply that all of them are not independent.

The definition of pair occupation operators can be generalized to multi-site occupation operators. Thus, the configuration of a triangle cluster consisting of the sites i, j, and k occupied by atoms of the type P, Q, and R, respectively, can be specified by the triangle occupation operator p_{ijk}^{PQR}, which is given by

$$p_{ijk}^{PQR} = p_i^P \bullet p_j^Q \bullet p_k^R \tag{4}$$

The triangle occupation operators also satisfy normalization and reduction constraints similar to those in Eqns. (2) and (3). Cluster occupation operators for tetrahedron and larger clusters of sites can be defined similarly.

To represent the configurational dependence of macroscopic properties such as energy, it is not necessary to specify the occupation of each cluster in the crystal. It is sufficient to specify the probabilities of occurrence of different clusters up to a chosen maximal cluster depending on the range of interactions occurring in the system. Cluster probabilities can be obtained by averaging the corresponding cluster occupation operators over all crystallographically equivalent clusters in the crystal. It follows that the averages of site occupation operators over all sites of the disordered crystal are equal to the respective mole fractions (also called point cluster variables).

$$x_P = \langle p_i^P \rangle \quad P = A,B\ldots Z \tag{5}$$

which satisfy the following conditions

$$0 \le x_P \le 1, \sum_{P=A}^{Z} x_P = 1 \tag{6}$$

Although only $(\kappa - 1)$ of the κ mole fractions are independent, we shall retain all of them in the description of the configuration of the alloy to obtain expressions that are symmetric in the components. This also necessitates the use of the constraint in Eqn. (6) when required. Similarly, the averages of pair occupation operators over all the crystallographically equivalent pairs of sites in the structure give the corresponding pair cluster probabilities or cluster variables ρ_{ij}^{PR}. Thus

$$\rho_{ij}^{PR} = \langle p_{ij}^{PR} \rangle = \langle p_i^P \bullet p_j^R \rangle \quad P,R = A,B\ldots Z \tag{7}$$

The cluster probabilities must also satisfy the following conditions

$$0 \le \rho_{ij}^{PR} \le 1, \sum_P \sum_R \rho_{ij}^{PR} = 1 \tag{8}$$

Further, they are related to the mole fractions through the reduction relations (also called sum rules) which follow from Eqn. (3)

$$\sum_R \rho_{ij}^{PR} = x_P \tag{9}$$

The total number of pair cluster variables is κ^2 for any chosen crystallographically distinct pair cluster. Owing to the crystallographic equivalence of all sites in disordered crystals, it follows from Eqn. (6) that

$$\rho_{ij}^{PR} = \rho_{ij}^{RP}, P \ne R \tag{10}$$

This reduces the number of distinct pair cluster variables to $\kappa(\kappa+1)/2$. In a similar manner, the number of distinct cluster variables could be reduced further in high-symmetry crystals such as bcc or fcc crystals. Only $\kappa(\kappa-1)/2$ of the distinct pair cluster variables are independent since only $(\kappa-1)$ site operators for each of the two sites are independent. The remaining κ cluster variables are dependent and can be expressed in terms of the set of independent pair and point cluster variables.

Cluster variables corresponding to crystallographically distinct clusters with an arbitrary number of sites, ν, can be defined in a similar manner. Normalization and geometric reduction rules, similar to those given by Eqns. (8) and (9) also apply to such cluster variables. The total number of ν-point CVs is κ^ν. However, only $(\kappa-1)^\nu$ of these are independent. The remaining $\kappa^\nu - (\kappa-1)^\nu$ CVs are dependent and can be expressed in terms of the set of independent ν-point CVs and those corresponding to the subclusters of the ν-point CV. Thus, a set of appropriately chosen $(\kappa-1)^\nu$ CVs constitutes a complete set of independent basis functions for the description of the alloy configuration, unlike the full set of κ^ν CVs. Note that the total number of distinct cluster variables as well as the number of distinct independent and dependent cluster variables, can be lower owing to symmetry. Such a distinct, independent, and complete set of CVs is a suitable basis for expanding the configurational properties of an alloy [41]. We shall designate the CVs of such a set or, in some cases, their simple linear combinations as correlation functions. This definition of correlation functions, like any currently used definition, is also not unique. The selection of CVs constituting the distinct, independent, and complete set of CVs to be designated as CFs is based on the criteria mentioned earlier.

2.2. Correlation functions for bcc phase

We shall now illustrate this approach for the disordered *bcc* phase (A2). Generally the smallest tetrahedron cluster in a structure will be treated as the basic cluster. For the bcc structure, this is the irregular tetrahedron cluster shown in Fig. 1. Clusters and sub−clusters used in tetrahedron approximation for bcc structure: point (1), I−n pair (12), II−n pair (13), triangle (123), and tetrahedron (1234).

It is not possible to choose a set of (κ - 1) independent point cluster variables as CFs while maintaining symmetry among the components. Further, point cluster interactions do not appear in the equilibrium equations, obviating the necessity of defining corresponding CFs. In view of these circumstances, we refrain from defining point cluster CFs and retain the entire set of point cluster variables in the description. Next, consider the pair cluster variables for one pair type (e.g., nearest neighbor pair). As mentioned earlier, the number of distinct and inde-

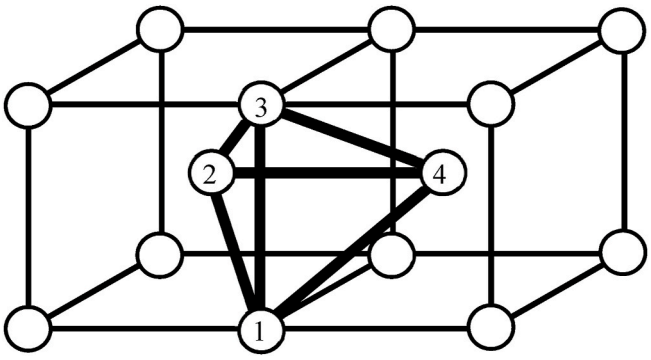

Fig. 1. Clusters and sub-clusters used in tetrahedron approximation for bcc structure: point (1), I−n pair (1−2), II−n pair (1−3), triangle (1−2−3), and tetrahedron (1−2−3−4).

pendent pair CVs is $\kappa(\kappa-1)/2$, while that of the distinct and dependent pair CVs is κ. In the case of disordered alloys, there are κ distinct pair cluster variables of the type ρ_{ij}^{PP} and $\kappa(\kappa-1)/2$ distinct pair cluster variables of the type $\rho_{ij}^{PR}, P \neq R$. Thus, CVs of the type $\rho_{ij}^{PR}, P \neq R$ correspond to the desired number of independent and distinct CVs for a description of the configurational state of a binary alloy or a binary subsystem of a multicomponent system and satisfy the conditions mentioned above for selection as CFs. Accordingly, we will define the I-neighbor ($v2PR1$) and II-neighbor ($v2PR2$) pair CFs as follows.

$$v2\ PR\ 1 = \rho_{12}^{PR} = \rho_{12}^{RP}, P < R \tag{11}$$

$$v2\ PR\ 2 = \rho_{13}^{PR} = \rho_{13}^{RP}, P < R \tag{12}$$

It remains only to show that CVs of the type ρ_{ij}^{PP} for I-n or II-n pair clusters can be expressed in terms of the chosen CFs. The sum in Eqn. (9) for kth neighbor pair clusters can be expressed as follows.

$$x_P = \sum_{X=A}^{Z} \rho_{ij}^{PX}(k) = \sum_{X=1}^{P-1} \rho_{ij}^{PX}(k) + \rho_{ij}^{PP}(k) + \sum_{X=P+1}^{Z} \rho_{ij}^{PX}(k)$$

Note that the dummy index X can be greater, equal, or lesser than P. Changing the dummy index in the two summations to conform to our notation convention, we have

$$\sum_{N=1}^{P-1} \rho_{ij}^{NP}(k) + \rho_{ij}^{PP}(k) + \sum_{Q=P+1}^{Z} \rho_{ij}^{PQ}(k) = x_P$$

On rearranging and using the definition of the pair CFs given above, we get

$$\rho_{ij}^{PP}(k) = x_P - \sum_{N=1}^{P-1} v2NPk - \sum_{Q=P+1}^{Z} v2PQk \quad k = 1, 2 \tag{13}$$

It may be seen that all the CVs have been expressed in terms of chosen point and pair CFs (Eqns. (11)–(13)).

The type (and number) of distinct triangle cluster configurations (sites 123 in Fig. 1) are PPP (κ), PPR or PRR ($\kappa(\kappa-1)$), PRP or RPR ($\kappa(\kappa-1)$) and RPT or PRT or PTR ($\kappa(\kappa-1)(\kappa-2)/2$) giving a total of $\kappa^2(\kappa+1)/2$ cluster configurations and thus CVs. It follows that the number of distinct and independent triangle CVs is $\kappa(\kappa-1)^2/2$. A subset of CVs numbering $\kappa(\kappa-1)^2/2$ must be chosen as CFs. It also follows that the number of distinct dependent triangle CVs is $\kappa(3\kappa-1)/2$. Clearly, CVs of the type ρ_{123}^{RPT} can occur only in ternary and higher-order systems. For each binary system and binary subsystem of a multicomponent system, we must choose 1 triangle CV (or combination of CVs) in which both components are present to be part of the independent set of CVs and thus designated as CFs for each such system. There are 4 such distinct CVs, namely $\rho_{123}^{PPR}, \rho_{123}^{PRR}, \rho_{123}^{PRP}, \rho_{123}^{RPR}, P < R$. None of them is symmetric in the two components. However, two distinct anti-symmetric combinations are possible: $\rho_{123}^{RPR} - \rho_{123}^{PRP}$ and $\rho_{123}^{PRR} - \rho_{123}^{PPR}$. Since only one such combination is required, an arbitrary choice must be made between the two possibilities. We shall choose the former here and call it $v3PR$.

$$v3\ PR = \rho_{123}^{RPR} - \rho_{123}^{PRP} \tag{14}$$

The number of such CFs is $\kappa(\kappa-1)/2$ since the number of CVs of the type PRP or RPR is $\kappa(\kappa-1)$. For ternary systems and ternary subsystems of multicomponent systems, we must choose another set of $\kappa(\kappa-1)^2/2 - \kappa(\kappa-1)/2 = \kappa(\kappa-1)(\kappa-2)/2$ distinct and independent CVs as CFs. Thus, for each ternary system and ternary subsystem of a multicomponent system, we must choose 3 additional triangle CVs (or combination of CVs) in which all three components are present to be part of the independent set of CVs and thus designated as CFs for each such system. There are just 3 such distinct CVs that can therefore be used to define the following triangle CFs.

$$v3PRT1 = \rho_{123}^{RPT}, v3PRT2 = \rho_{123}^{PRT}, v3PRT3 = \rho_{123}^{PTR} \tag{15}$$

All the dependent triangle CVs can be expressed in terms of these CFs using appropriate sum rules for the triangle CVs. The solutions are given below.

$$\rho_{123}^{PPR} = \frac{1}{2}\Bigg[v2\ PR\ 2 - v3\ PR + \sum_{N=A}^{P-1}(- v3NPR1 - v3NPR2 + v3NPR3) + \sum_{Q=P+1}^{R-1}(- v3PQR1 - v3PQR2 + v3PQR3) + \sum_{S=R+1}^{Z}(- v3PRS1 + v3PRS2 - v3PRS3)\Bigg] \tag{16}$$

$$\rho_{123}^{PRR} = \frac{1}{2}\Bigg[v2\ PR\ 2 + v3\ PR + \sum_{N=A}^{P-1}(- v3NPR1 + v3NPR2 - v3NPR3) + \sum_{Q=P+1}^{R-1}(v3PQR1 - v3PQR2 - v3PQR3) + \sum_{S=R+1}^{Z}(v3PRS1 - v3PRS2 - v3PRS3)\Bigg] \tag{17}$$

$$\rho_{123}^{PRP} = \frac{1}{2}\Bigg[2v2\ PR\ 1 - v2\ PR\ 2 - v3\ PR + \sum_{N=A}^{P-1}(v3NPR1 - v3NPR2 - v3NPR3) + \sum_{Q=P+1}^{R-1}(- v3PQR1 + v3PQR2 - v3PQR3) + \sum_{S=R+1}^{Z}(- v3PRS1 - v3PRS2 + v3PRS3)\Bigg] \tag{18}$$

$$\rho_{123}^{RPR} = \frac{1}{2}\Bigg[2v2\ PR\ 1 - v2\ PR\ 2 + v3\ PR + \sum_{N=A}^{P-1}(v3NPR1 - v3NPR2 - v3NPR3) + \sum_{Q=P+1}^{R-1}(- v3PQR1 + v3PQR2 - v3PQR3) + \sum_{S=R+1}^{Z}(- v3PRS1 - v3PRS2 + v3PRS3)\Bigg] \tag{19}$$

$$\rho_{123}^{PPP} = x_P - \frac{1}{2}\sum_{M=A}^{P-1}(2v2MP1 + v2MP2 + v3MP) - \frac{1}{2}\sum_{R=P+1}^{Z}(2v2\ PR\ 1 + v2\ PR\ 2 - v3\ PR) + \frac{1}{2}\left(\sum_{M=A}^{P-2}\sum_{N=M+1}^{P-1} v3MNP3 + \sum_{N=A}^{P-1}\sum_{S=P+1}^{Z} v3NPS2 + \sum_{S=P+1}^{Z-1}\sum_{T=S+1}^{Z} v3PST1\right) \quad (20)$$

We shall not give a detailed explanation for the choice of independent tetrahedron CVs from amongst all the CVs but only outline the results. For each binary system or binary subsystem of a higher-order system, one tetrahedron CV, namely, $\rho_{1234}^{PRPR} = \rho_{1234}^{RPRP}, P \neq R$ is chosen to be the tetrahedron CF designated *v4PQ*.

$$v4\ PR = \rho_{1234}^{PRPR} \quad (21)$$

Similarly, for each ternary system or ternary subsystem of a higher-order system, three tetrahedron CVs, namely, $\rho_{1234}^{PRPT}, \rho_{1234}^{PRTR}, \rho_{1234}^{PTRT}, P \neq R \neq T$ are chosen to be the tetrahedron CFs designated *v4PRT*1, *v4PRT*2, and *v4PRT*3, respectively.

$$v4PRT1 = \rho_{1234}^{PRPT};\ \ v4PRT2 = \rho_{1234}^{PRTR};\ \ v4PRT3 = \rho_{1234}^{PTRT} \quad (22)$$

Finally, for each quaternary system or quaternary subsystem of a higher-order system, three tetrahedron CVs, namely, $\rho_{1234}^{MRPT}, \rho_{1234}^{MPRT}, \rho_{1234}^{MPTR}$, $M \neq P \neq R \neq T$ are chosen to be the tetrahedron CFs designated *v4MRPT*1, *v4MRPT*2, and *v4MRPT*3, respectively.

$$v4MPRT1 = \rho_{1234}^{MRPT};\ \ v4MPRT2 = \rho_{1234}^{MPRT};\ \ v4MPRT3 = \rho_{1234}^{MPTR} \quad (23)$$

As in the case of triangle CFs, it can be easily shown that all dependent tetrahedron CVs can be expressed in terms of these CFs using appropriate tetrahedron CV sum rules. The solutions are given below.

$$\rho_{1234}^{PPPP} = x_P - \sum_{M=A}^{P-1}(2v2MP1 + v3MP - v4MP) - \sum_{R=P+1}^{Z}(2v2\ PR\ 1 - v3\ PR - v4\ PR) + 2\sum_{M=A}^{P-2}\sum_{N=M+1}^{P-1}(v3MNP3 + v4MNP3) + 2\sum_{N=A}^{P-1}\sum_{S=P+1}^{Z}(v3NPS2 + v4NPS2) + 2\sum_{S=P+1}^{Z-1}\sum_{T=S+1}^{Z}(v3PST1 + v4PST1) \quad (29)$$

There are no other types of CFs for any quinary or higher-order system since the basic cluster has been chosen to be the smallest tetrahedron which has only four sites. Table 1 summarises these results.

Correlation functions and cluster variable expressions for disordered fcc and hcp structures are given in Appendix 1 and 2, respectively.

2.3. Configurational enthalpy

Any function of configuration, such as the configurational enthalpy H_{mc} for a phase, can be expressed as a bilinear sum of the products of the correlation function (*v*1*PQ* … *v*13*PQRS*), and the respective cluster expansion coefficient (CEC, *e*, including the effect of multiplicity) [1, 42]. Thus

$$\rho_{1234}^{PPPR} = \frac{1}{2}\left[(2v2\ PR\ 1 - v2\ PR\ 2 - v3\ PR - 2v4\ PR) + \sum_{M=A}^{P-1}(v3MPR1 - v3MPR2 - v3MPR3 - 2v4MPR2) + \sum_{Q=P+1}^{R-1}(\right.$$
$$\left. - v3PQR1 + v3PQR2 - v3PQR3 - 2v4PQR1) + \sum_{T=R+1}^{Z}(-v3PRT1 - v3PRT2 + v3PRT3 - 2v4PRT1)\right] \quad (24)$$

$$\rho_{1234}^{PRRR} = \frac{1}{2}\left[(2v2\ PR\ 1 - v2\ PR\ 2 + v3\ PR - 2v4\ PR) + \sum_{M=A}^{P-1}(v3MPR1 - v3MPR2 - v3MPR3 - 2v4MPR3) + \sum_{Q=P+1}^{R-1}(\right.$$
$$\left. - v3PQR1 + v3PQR2 - v3PQR3 - 2v4PQR3) + \sum_{T=R+1}^{Z}(-v3PRT1 - v3PRT2 + v3PRT3 - 2v4PRT2)\right] \quad (25)$$

$$\rho_{1234}^{PPRT} = \frac{1}{2}\left[(-v3PRT1 + v3PRT2 + v3PRT3) + (v4PRT1 - v4PRT2 - v4PRT3) + \sum_{M=1}^{P-1}(v4MPRT1 - v4MPRT2 - v4MPRT3)\right.$$
$$+ \sum_{Q=P+1}^{R-1}(v4PQRT1 - v4PQRT2 - v4PQRT3) + \sum_{S=R+1}^{T-1}(-v4PRST1 + v4PRST2 - v4PRST3) \quad (26)$$
$$\left. + \sum_{U=T+1}^{Z}(-v4PRTU1 - v4PRTU2 + v4PRTU3)\right]$$

$$\rho_{1234}^{PRRT} = \frac{1}{2}\left[(v3PRT1 - v3PRT2 + v3PRT3) + (-v4PRT1 + v4PRT2 - v4PRT3) + \sum_{M=1}^{P-1}(-v4MPRT1 + v4MPRT2 - v4MPRT3) + \sum_{Q=P+1}^{R-1}(\right.$$
$$\left. - v4PQRT1 - v4PQRT2 + v4PQRT3) + \sum_{S=R+1}^{T-1}(-v4PRST1 - v4PRST2 + v4PRST3) + \sum_{U=T+1}^{Z}(v4PRTU1 - v4PRTU2 - v4PRTU3)\right] \quad (27)$$

$$\rho_{1234}^{PRTT} = \frac{1}{2}\left[(v3PRT1 + v3PRT2 - v3PRT3) + (-v4PRT1 - v4PRT2 + v4PRT3) + \sum_{M=1}^{P-1}(-v4MPRT1 - v4MPRT2 + v4MPRT3) + \sum_{Q=P+1}^{R-1}(\right.$$
$$\left. - v4PQRT1 + v4PQRT2 - v4PQRT3) + \sum_{S=R+1}^{T-1}(v4PRST1 - v4PRST2 - v4PRST3) + \sum_{U=T+1}^{Z}(v4PRTU1 - v4PRTU2 - v4PRTU3)\right] \quad (28)$$

Table 1
CFs for CE using tetrahedron approximation for bcc structure. Note that M < P < R < T.

System	Binary		Ternary		Quaternary	
Cluster Type	CF	No. of CF	CF	No. of CF	CF	No. of CF
Tetrahedron (1234)	*v*4 *PR*	1	*v*4 *PR*, …	3	*v*4 *PR*, …	6
			*v*4*PRT*1	1	*v*4*PRT*1, …	4
			*v*4*PRT*2	1	*v*4*PRT*2, …	4
			*v*4*PRT*3	1	*v*4*PRT*3, …	4
					*v*4*MPRT*1	1
					*v*4*MPRT*2	1
					*v*4*MPRT*3	1
Triangle (123)	*v*3 *PR*	1	*v*3 *PR*, …	3	*v*3 *PR*, …	6
			*v*3*PRT*1	1	*v*3*PRT*1, …	4
			*v*3*PRT*2	1	*v*3*PRT*2, …	4
			*v*3*PRT*3	1	*v*3*PRT*3, …	4
II-n Pair (13)	*v*2 *PR* 2	1	*v*2 *PR* 2, …	3	*v*2 *PR* 2, …	6
I-n Pair (12)	*v*2 *PR* 1	1	*v*2 *PR* 1, …	3	*v*2 *PR* 1, …	6
Point (1)	*xP*	1	*xP*, …	2	*xP*, …	3
Total no. of CFs		5		20		54

$$H_{mc} = \sum_{P=A}^{Y}\sum_{Q=P+1}^{Z}(e21PQ \bullet v21PQ + e22PQ \bullet v22PQ + e3PQ \bullet v3PQ + e4PQ \bullet v4PQ) + \sum_{P=A}^{X}\sum_{Q=P+1}^{Y}\sum_{R=Q+1}^{Z}(e3PQR1 \bullet v3PQR1 + e3PQR2 \bullet v3PQR2 + e3PQR3 \bullet v3PQR3 + e4PQR1 \bullet v4PQR1 + e4PQR2 \bullet v4PQR2 + e4PQR3 \bullet v4PQR3) + \sum_{P=A}^{W}\sum_{Q=P+1}^{X}\sum_{R=Q+1}^{Y} \times \sum_{S=R+1}^{Z}(e4PQRS1 \bullet v4PQRS1 + e4PQRS2 \bullet v4PQRS2 + e4PQRS3 \bullet v4PQRS3) \quad (30)$$

where, $P,Q,R,S \in \{A,B,C,D,\ldots,W,X,Y,Z\}$.

The first summation pertains to a binary system or all binary subsystems of a higher-order system. The second summation pertains to a ternary system or all ternary subsystems of a higher-order system. Finally, the last summation pertains to a quaternary system or all quaternary subsystems of a higher-order system. Since these summations contain terms for binary, ternary, or quaternary systems, respectively, independent of whether they are subsystems of a higher-order system, it follows that all the CECs remain unchanged or can be inherited from any lower-order system to a higher-order system. No other configurational description available in the literature has this feature.

Further, the cluster expansion for quinary and higher-order systems does not involve any additional CECs besides those of all its quaternary subsystems. This has two significant implications: (i) there is no exponential increase in the number of CFs and CECs for multi-component alloys, which is contrary to general belief, and (ii) databases such as those for standard CALPHAD methods can be constructed for CE-CVM. These conclusions implicitly assume that the same maximal cluster is used for all systems and subsystems in the CE. The choice of the maximal cluster to be used in general can be inferred indirectly from the large amount of literature available on an optimal number of terms in Redlich-Kister type expansions used in CALPHAD. Zhang and Sluiter [29] have discussed the issue of the choice of an optimal maximal cluster (or set of clusters) for *fcc* alloys in detail. They have used two criteria for this choice: (i) clusters consisting only of 4 sites and their subclusters are considered, and (ii) clusters with only up to 8th nearest-neighbor pairs are considered. They have justified these criteria based on results of fitting of phase diagrams available in the literature using a CALPHAD type approach. These results have shown that fourth-order polynomials in the composition are able to represent the enthalpy of mixing with sufficient accuracy. Therefore, multiatom interactions in clusters with up to only 4 sites should be sufficient to represent the enthalpy in a cluster expansion. Further, Zhang and Sluiter [29] have argued that all observed *fcc* based superstructures, with the exception of long-period superstructures, can be stabilized by pair-wise interactions up to the 8th nearest neighbors. The $D0_{23}$ structure observed in Al_3Zr requires the latter interactions for stabilization. However, the $D0_{23}$ structure can be more appropriately considered to be part of the family of long period superstructures such as $D0_{22}$ (prototype Al_3Ti) which require to be treated by a completely different approach. Similarly, the treatment of coherent precipitates such as GP zones needs separate consideration. Leaving such cases aside, interactions up to 2nd neighbor pairs should suffice. There is only one such maximal cluster, namely, the irregular tetrahedron shown in Fig. 1, for the *bcc* structure.

Table 2
Optimized set of CECs for the Nb-Ti system.

Phase	Parameters (J/mol)
bcc phase	$E21NbTi = -390$ (I-neighbor pair)
	$E22NbTi = -260$ (II-neighbor pair)
	$E3PQ = 0$ (triangle)
hcp	$E21NbTi = -281$ (I-neighbor pair)
	$E22NbTi = -281$ (II-neighbor pair)
Liquid	$L_0^l = 3466$

2.4. Cluster variation method

The expression for the configurational entropy of mixing per mole is given by (Kikuchi, 1951)

$$S_{mc} = -R\sum_{j=1}^{\alpha} m_j\gamma_j \sum_{\sigma_j}\rho_j(\sigma_j)\ln\rho_j(\sigma_j) \quad (31)$$

where $\rho_j(\sigma_j)$ represents a cluster variable for j cluster corresponding to the configuration denoted by σ_j. In the above expression, the cluster variables $\rho_j(\sigma_j)$ can be expressed as functions of correlation functions v_k, i.e., $\rho_j(\sigma_j) = \rho_j(\sigma_j)(v_k)$ as shown above. The m_j represent the multiplicity of clusters of type j and are equal to the number of such clusters per site in the structure. Here the γ_j represent the overlap correction coefficients and are referred to as Kikuchi−Barker (K–B) coefficients. By definition, $\gamma_\alpha = 1$. Values of the K-B coefficients are given, for example, by Sarma et al. [34]. It may be noted that the above expression corresponds to the total configurational entropy of mixing and not just the excess entropy of mixing.

The configurational contribution to the Gibbs energy of mixing is thus given by

$$G_{mc} = H_{mc} + RT\sum_{j=1}^{\alpha} m_j\gamma_j \sum_{\sigma_j}\rho_j(\sigma_j)\ln\rho_j(\sigma_j)(v_k) \quad (32)$$

Gibbs energy needs to be minimized, after substituting CVs in terms of CFs, with respect to correlation functions, to obtain an equilibrium configuration.

After substituting for the multiplicity, the configurational Gibbs en-

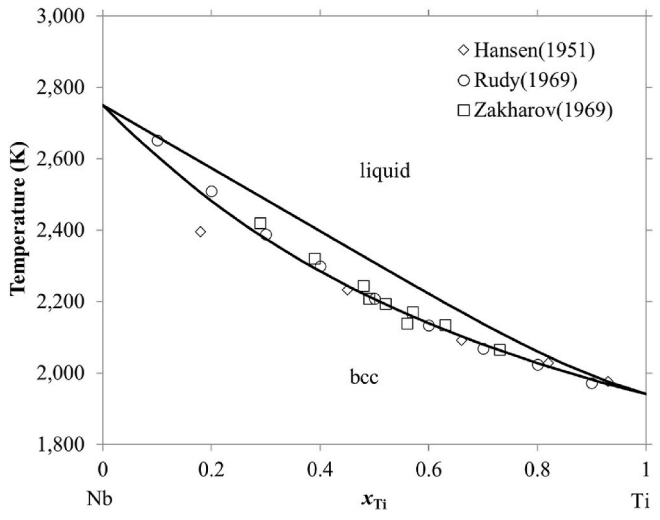

Fig. 2. Calculated liquidus and solidus boundaries of the Nb-Ti system along with experimental data.

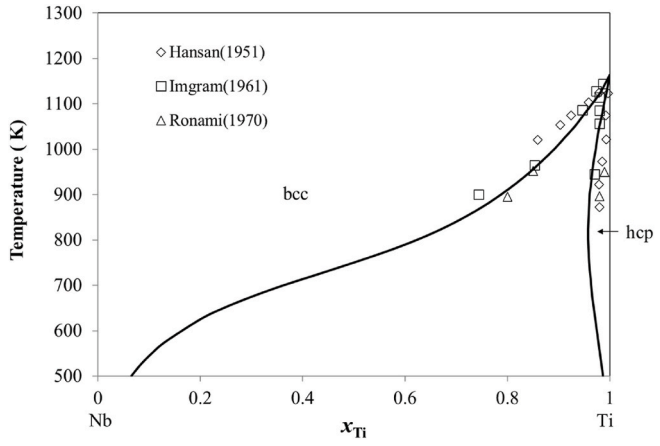

Fig. 3. Calculated solvus boundaries of the Nb-Ti System along with experimental data.

ergy of mixing for a bcc phase in a quaternary system is given by

$$G_{mc} = e2\,PR\,1 \bullet v2\,PR\,1 + e2\,PR\,2 \bullet v2\,PR\,2 + e3\,PR \bullet v3\,PR + e4\,PR \bullet v4\,PR + RT\big(6.\big(\rho_{1234}^{PPPP}\ln\rho_{1234}^{PPPP} + 4\rho_{1234}^{PPPR}\ln\rho_{1234}^{PPPR} + 4\rho_{1234}^{PRRR}\ln\rho_{1234}^{PRRR} + 2\rho_{1234}^{PRPR}\ln\rho_{1234}^{PRPR} + 4\rho_{1234}^{PPRR}\ln\rho_{1234}^{PPRR} + \rho_{1234}^{RRRR}\ln\rho_{1234}^{RRRR}\big) - 12.\big(\rho_{123}^{PPP}\ln\rho_{123}^{PPP} + \rho_{123}^{PRP}\ln\rho_{123}^{PRP} + 2\rho_{123}^{PPR}\ln\rho_{123}^{PPR} + 2\rho_{123}^{PRR}\ln\rho_{123}^{PRR} + \rho_{123}^{RPR}\ln\rho_{123}^{RPR} + \rho_{123}^{RRR}\ln\rho_{123}^{RRR}\big) + 3.\big(\rho_{13}^{PP}\ln\rho_{13}^{PP} + 2\rho_{13}^{PR}\ln\rho_{13}^{PR} + \rho_{13}^{RR}\ln\rho_{13}^{RR}\big) + 4.\big(\rho_{12}^{PP}\ln\rho_{12}^{PP} + 2\rho_{12}^{PR}\ln\rho_{12}^{PR} + \rho_{12}^{RR}\ln\rho_{12}^{RR}\big) - 1.(xP\ln xP + xR\ln xR)\big) \quad (33)$$

2.5. Thermodynamic assessments and calculations

For the thermodynamic assessment of the binary systems, we

Table 3
Optimized set of CECs for the Nb-V system.

Phase	Parameters (J/mol)
bcc phase	$E21NbV = -880$ (I-neighbor pair) $E22NbV = -586.67$ (II-neighbor pair) $E3NbTi = 0$ (triangle)
Liquid	$L_0^l = -11400 + 10{*}T$

Table 4
Invariant points in the Nb-V phase diagram.

Invariants	T(K)	x_V
Congruent Minimum	2132.7	0.797
Consolute Point	1076.5	0.5

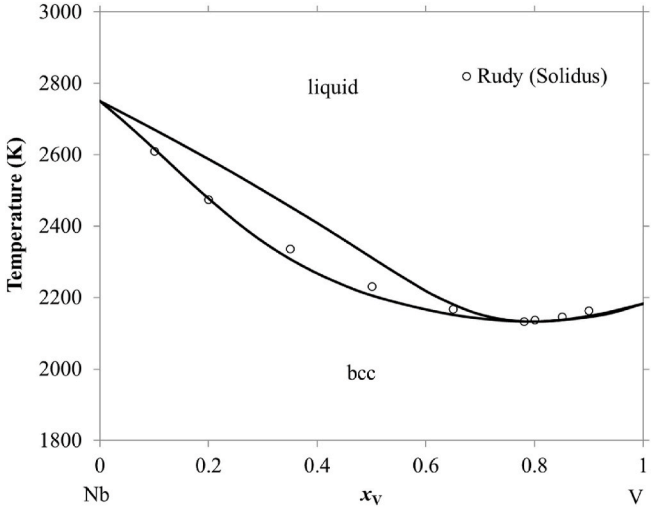

Fig. 4. Calculated liquidus and solidus boundaries of the Nb-V system along with experimental data [47].

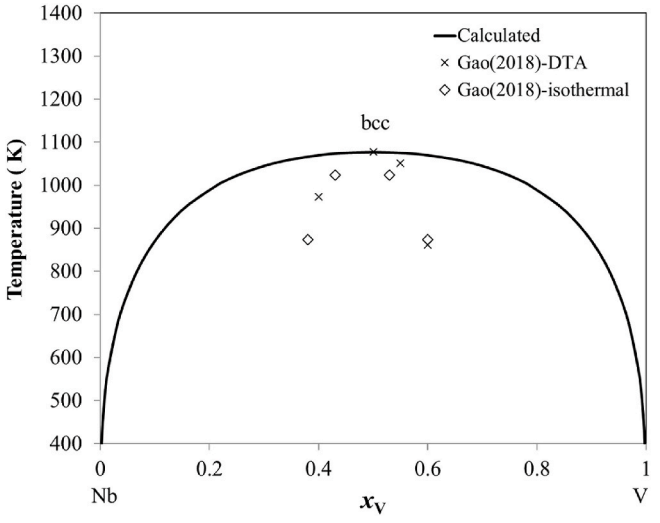

Fig. 5. Calculated miscibility gap in the bcc phase (solid line) of the Nb-V system along with experimental data [47].

Table 5
Optimized set of CECs for the Nb-Zr system.

Phase	Parameters (J/mol)
bcc phase	$E21NbZr = -462.6 - 0.4152{*}T$ (I-neighbor pair) $E22NbZr = -308.4 - 0.2768{*}T$ (II-neighbor pair) $E3NbZr = 88.0$ (Triangle)
hcp	$E21NbZr = -841.4$ (I-neighbor pair) $E22NbZr = -841.4$ (II-neighbor pair)
Liquid	L_0^l = -41300.0 + 28*T L_1^l = -23150.0 + 10*T

Table 6
Invariant points in the Nb-Zr phase diagram.

Invariants	T(K)	x_{Zr}
Congruent Minimum	2023	0.742
Consolute Point	1245	0.412
Monotectoid	895	0.074 (βNb)
		0.797 (βZr)
		0.986 (αZr)

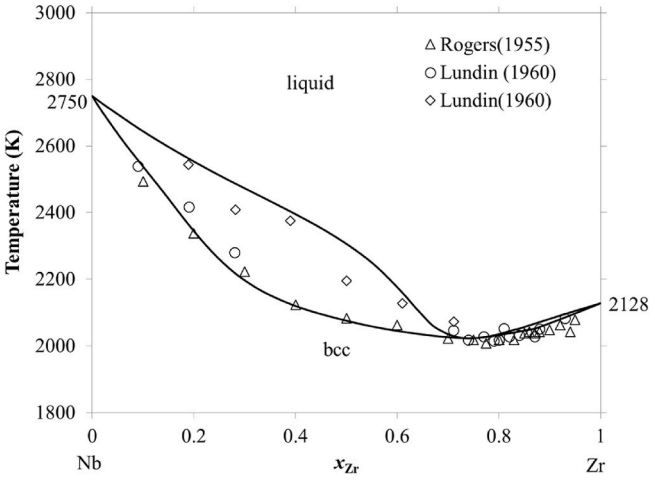

Fig. 6. Calculated liquidus and solidus boundaries in the Nb-Zr system along with experimental data [46].

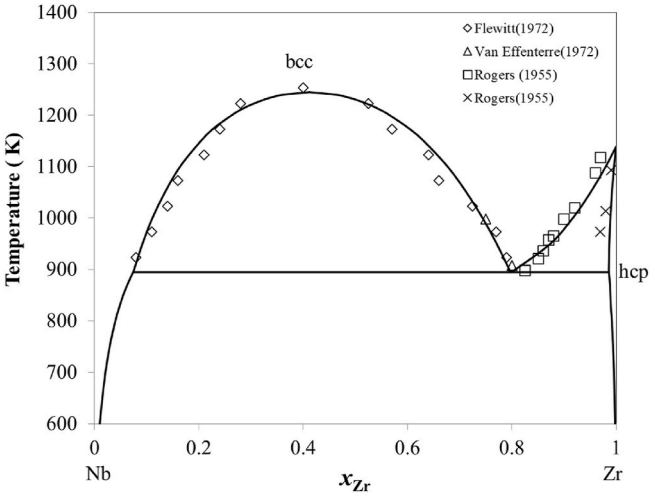

Fig. 7. Calculated miscibility gap and monotectiod reaction in the solid phase (solid line) along with experimental data [46].

Table 7
Optimized set of CECs for the Ti-V system.

Phase	Parameters (J/mol)
bcc phase	$E21TiV = -510$ (I-neighbor pair)
	$E22TiV = -340$ (II-neighbor pair)
	$E3TiV = 0$ (triangle)
hcp	$E21TiV = -770$ (I-neighbor pair)
	$E22TiV = -770$ (II-neighbor pair)
Liquid	$L_0^l = 5900$
	$L_1^l = 1510$

employed the Levenberg–Marquardt (LM) algorithm to optimize model parameters in the outermost loop. The Newton-Raphson method was used in two internal loops: (i) for calculating phase boundaries and (ii) for the internal minimization of the CE-CVM expressions. Further details on these calculations can be found in our previous publications [43]. We have adapted Hillert's [44,45] algorithm for both phase boundary calculations and the internal minimization of CE-CVM expressions for thermodynamic calculations related to higher-order systems. We will be publishing the details of these algorithms in a separate publication.

3. Nb-Ti-V-Zr system

A scheme to obtain an optimized set of CECs for a quaternary system will be demonstrated in this section. We will use optimized model parameters where such parameters are already available in the literature. If required, optimization of the binary and ternary sub-systems will be undertaken. Since our focus here is on demonstrating the development of multi-component cluster expansion for the disordered bcc phase, details of the thermodynamics of other phases (such as liquid and hcp) will be limited. Most of the available parameters are in the form of Redlich-Kister parameters. A method to transform them to yield initial estimates of CECs is presented in Appendix 3. The optimized model parameters for many binary subsystems have been previously reported in our earlier works [46–48]. These parameters (CECs) were originally presented using a conventional orthogonal basis. In Section 3.1, we provide these values with additional fine-tuning, where necessary. The corresponding CECs in the CVCF basis, developed in this work, were obtained by transforming the orthogonal basis CECs using the procedure detailed in Appendix 4.

3.1. Binary subsystems

3.1.1. Nb-Ti system

The equilibrium diagram of the system has been studied by Kaufman and Bernstein [49], Murray et al. [50,51], Kumar et al. [52], and Zhang et al. [53]. Assessed values of CECs for this system were obtained by Refs. [48,54]. The system was re-optimized in this work to reproduce experimental data better (see Table 2 and Figs. 2 and 3). All experimental data, cited in Ref. [53], are used for this optimization except the first principles thermochemical data.

3.1.2. Nb-V system

Many researchers have computed the Nb-V phase diagram based on available experimental data. Molokanov et al. [55], Balakrishna and Mallik [56], and Smith et al. [57] calculated the Nb-V phase diagram and obtained similar results as shown by Rudy [58]. Further, Kumar et al. [52] studied the Nb-Ti-V phase diagram and re-optimized the Nb-V system. Recently, Gao et al. [59] have reassessed this phase diagram based on their new experimental results. Different orders of Redlich-Kister polynomials [36] were used in these works to model the phases present. Shanker et al. [47] have optimized this system using CE-CVM for the bcc phase. We will use the CEC values for the bcc phase obtained in this study further in this work (see Tables 3 and 4 and Figs. 4 and 5).

3.1.3. Nb-Zr system

Thermodynamic assessment of the Nb-Zr system has been done by Abriata et al. [60], Guillermet et al. [61], Lafaye et al. [62]. CE-CVM-based description of the bcc phases has become available recently [46]. We will use the CEC values for the bcc phase obtained in

Table 8
Invariant point in the Ti-V phase diagram.

Invariant(s)	T(K)	x_V
Congruent Minimum	1881	0.333

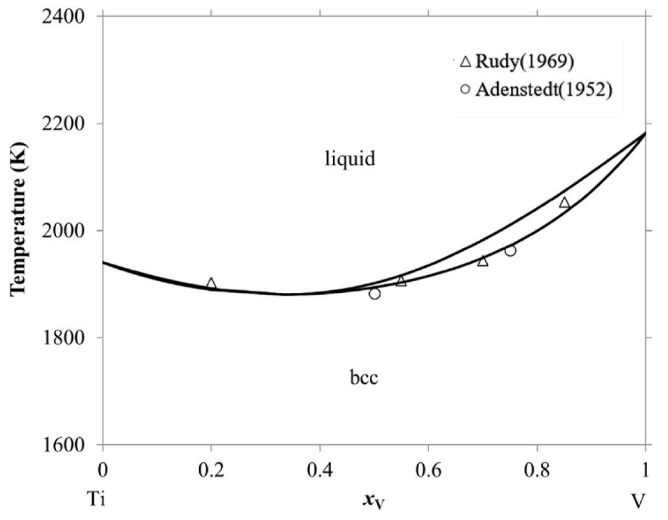

Fig. 8. Calculated liquidus and solidus boundaries of the Ti-V system along with experimental data.

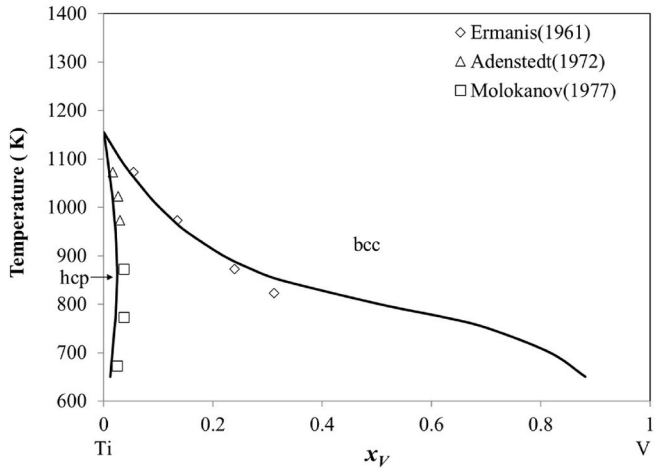

Fig. 9. Calculated solvus boundaries of the Ti-V System along with experimental data.

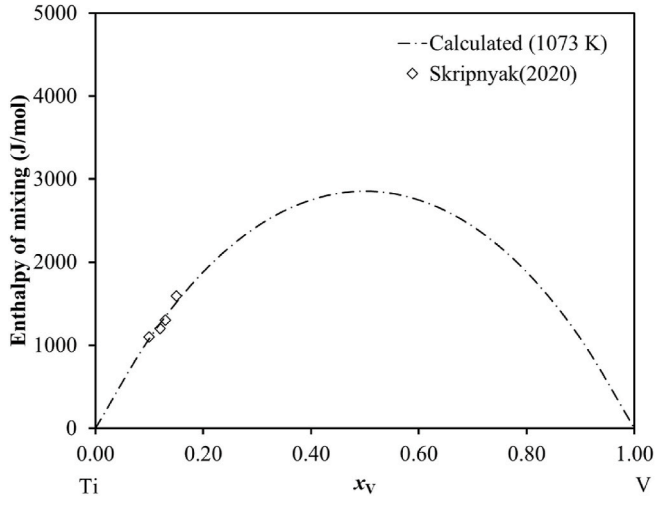

Fig. 10. Calculated enthalpy of mixing for the bcc phase at 1073K (chain line) of the Ti-V system along with experimental data of Skripnyak et al. [66].

Table 9
Optimized set of CECs for the Ti-Zr system.

Phase	Parameters (J/mol)
bcc	$E21TiZr = 579$ (I-neighbor pair) $E22TiZr = 386$ (II-neighbor pair) $E3TiZr = 0$ (triangle)
hcp	$E21TiZr = 216 + 0.202*T$ (I-neighbor pair) $E22TiZr = 216 + 0.202*T$ (II-neighbor pair)
Liquid	$L_0^l = 21219$

Table 10
Invariant points in the Ti-Zr system.

Invariants	T(K)	x_{Zr}
Congruent (liquid ↔ bcc)	1811.7	0.352
Congruent (bcc↔ hcp)	875.4	0.503

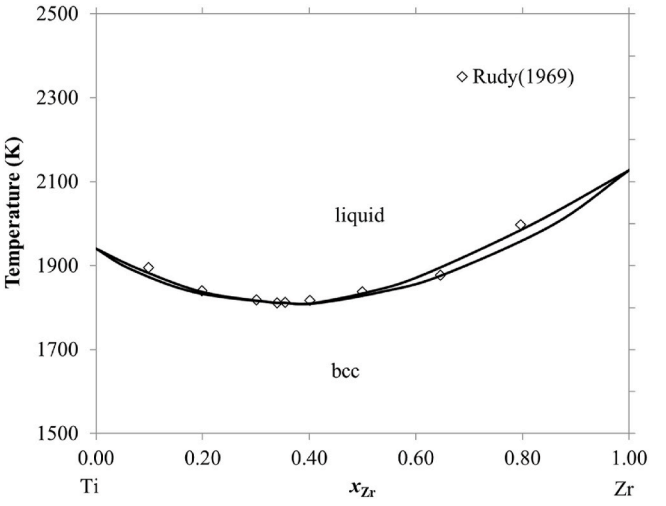

Fig. 11. Calculated liquidus and solidus boundaries of the Ti-Zr system along with experimental data.

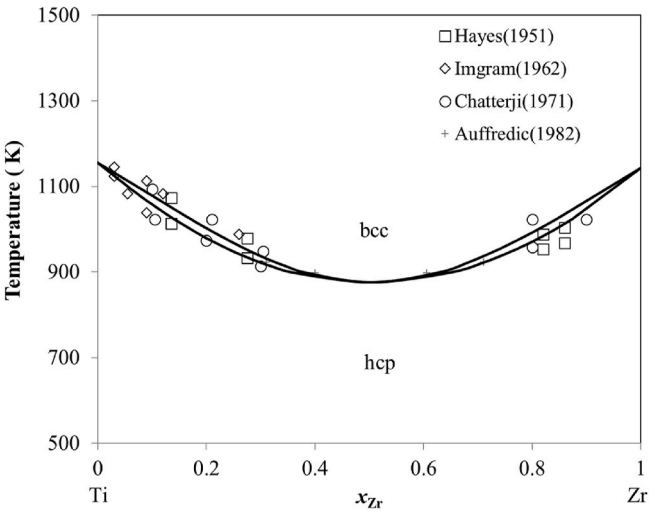

Fig. 12. Calculated solvus boundaries of the Ti-Zr system along with experimental data.

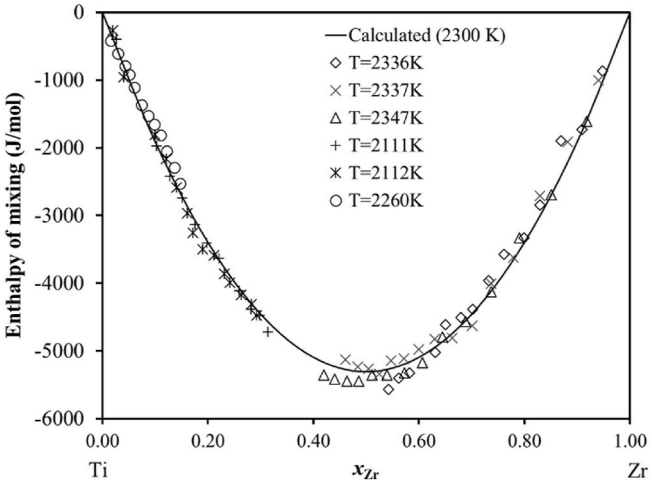

Fig. 13. Calculated enthalpy of mixing for the liquid phase at 2300 K (solid line) of the Ti-Zr system along with experimental data of Thiedemann et al. [71] at various temperatures.

Table 11
Optimized set of CECs for the V-Zr system.

Phase	Parameters (J/mol)
bcc	$E21VZr = -1120 - 0.159T$ (I-neighbor pair) $E22VZr = -746.7 - 0.106T$ (II-neighbor pair) $E3VZr = 120$ (triangle)

Table 12
Invariant points in the V-Zr system.

Invariants	Experimental data		This work (Calculated)	
	T(K)	x_{Zr}	T(K)	x_{Zr}
Peritectic	1585[a]	–	1587	0.075 (bcc)
	1573[b]	–		0.334 (Laves_C15)
		0.42 (liquid)[a]		0.412 (liquid)
Eutectic	1537[a]	–	1538.7	0.355(Laves_C15)
	1503[b]	0.54 (liquid)[a]		0.539 (liquid)
		–		0.824 (bcc)
Eutectoid	1070[a]	–	1072	0.35 (Laves_C15)
	1050[b]	–		0.953(bcc)
		–		0.988(hcp)

[a] [76].
[b] [77].

this study further in this work (see Tables 5 and 6 and Figs. 6 and 7).

3.1.4. Ti-V system

The binary Ti-V system is a simple system with no intermediate phase. The Ti–V system was optimized by Murray [63], Saunders [64], and Ghosh [65]. Shanker et al. [48] have optimized this system using CE-CVM for the bcc phase. This system is re-optimized by considering a simplified CE-CVM description to model the bcc phase using experimental and theoretical data considered in Ref. [48] (see Tables 7 and 8 and Figs. 8–10).

3.1.5. Ti-Zr system

The phase diagram of Ti-Zr consists of three phases liquid, hcp(α), and bcc(β) and shows complete solubility in all three phases. Thermodynamic assessments of this system have been given by Murray [67], Hari Kumar et al. [68], Turchanin et al. [69], and Cui [70]. The studies of Murray [67] and Hari Kumar et al. [68] did not consider the mixing enthalpy of the liquid alloys [71] in the Ti–Zr system. Later, Sridar et al. [72] revised their assessment by considering the enthalpy of mixing of

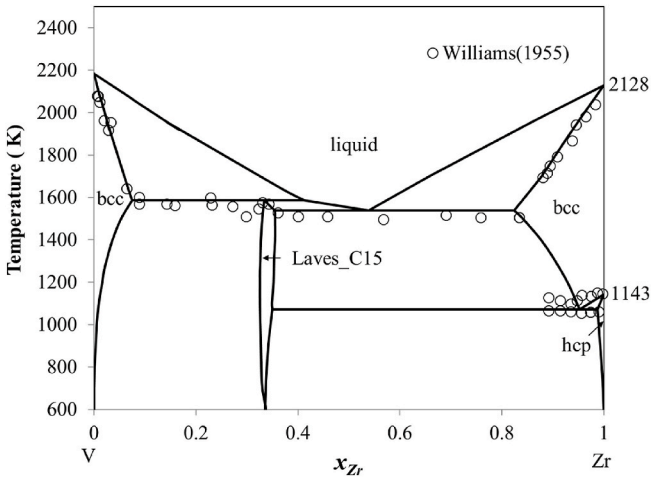

Fig. 14. Calculated phase diagram of the V-Zr system along with experimental data from [77].

Table 13
Optimized set of CECs for the Nb-Ti-V system.

Phase	Parameters (J/mol)
bcc phase	e3NbTiV1 = e3NbTiV2 = e3NbTiV3 = − 20000. e4NbTiV1 = 48800 e4NbTiV2 = − 24400. e4NbTiV3 = − 24400

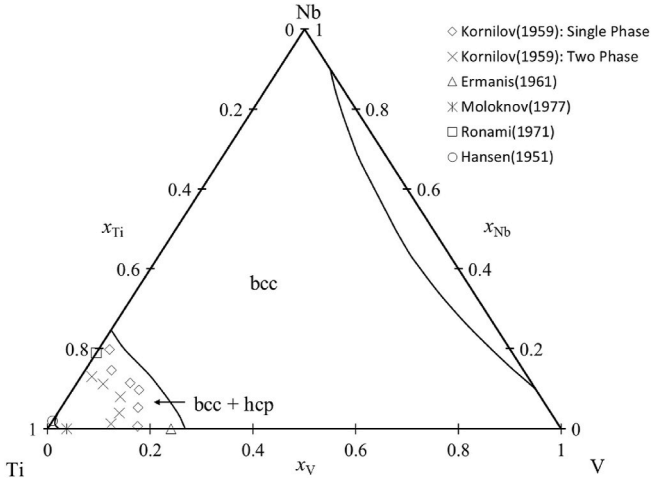

Fig. 15. Calculated isothermal section of Nb-Ti-V system at 873 K showing miscibility gap boundary.

the liquid phase. Shanker et al. [48] have optimized this system using CE-CVM for the bcc phase. This system is re-optimized here to improve CECs for the bcc phase (see Tables 9 and 10 and Figs. 11–13).

3.1.6. V-Zr system

This system exhibits an intermediate phase V_2Zr (Laves_C15), which melts incongruently by a peritectic reaction $V_2Zr \rightarrow$ Liquid + bcc(V). The

Table 14
Optimized set of CECs for the Nb-Ti-Zr system.

Phase	Parameters (J/mol)
bcc phase	e3NbTiZr1 = e3NbTiZr2 = e3NbTiZr3 = − 3333.33. e4NbTiZr1 = 0 e4NbTiZr2 = 0. e4NbTiZr3 = 0

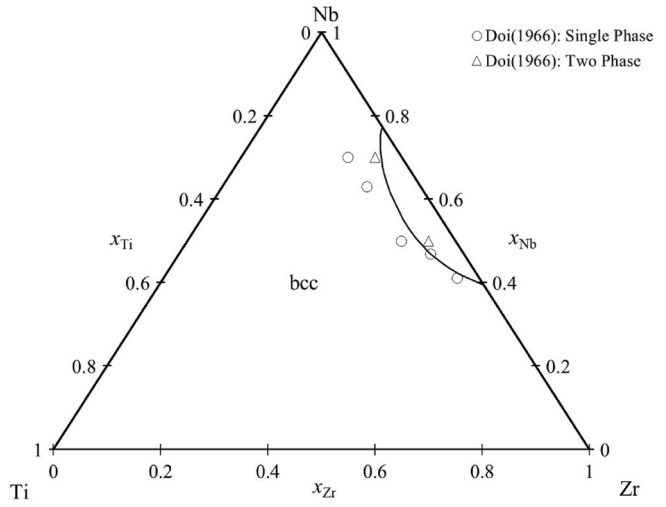

Fig. 16. Calculated isothermal section of Nb-Ti-Zr system at 1173 K showing miscibility gap boundary along with experimental data from Ref. [84].

V–Zr system was first modeled by Korb et al. [73]. Later, the V–Zr system was optimized by Servant [74], Zhao et al. [75], and Cui et al. [70,76]. For the present work, we have accepted the latest parameters from Cui et al. [70,76] for all the phases except bcc. The system was optimized considering all the available experimental data and treating the bcc phase within the CE-CVM framework (see Tables 11 and 12 and Fig. 14).

3.2. Ternary subsystems

3.2.1. Nb-Ti-V system

Kornilov and Vlasov studied this system at 873 and 973 K [78]. Komjathy [79] concluded that a continuous series of bcc solid solutions is formed above 1073 K. This system has been reviewed by Enomoto [80]. The thermodynamic descriptions of the bcc Ti-Nb-V ternary system have been reported by Kumar et al. [52], Lee et al. [81], Wei et al. [82] and Hu et al. [83]. Kumar et al. [52] did not consider ternary interaction parameters in their calculations. Wei et al. [82] have obtained ternary interaction parameters considering the binary miscibility gap in the Nb-V system [59] and experimental data [78]. We have accepted their thermodynamic description of the Nb-Ti-V system in this work and optimized the corresponding CEC parameters to reproduce the miscibility gap in the bcc phase, as reported by them [82]. Optimized

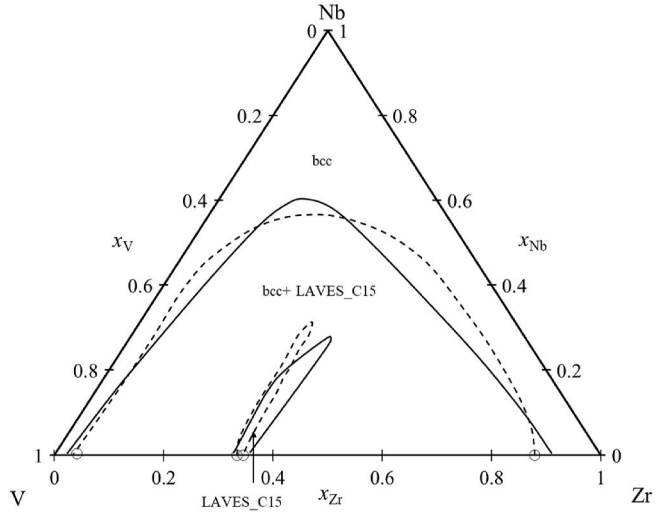

Fig. 17. Calculated isothermal section of the Nb-V-Zr system at 1273 K. The dashed lines (–) represent the phase boundaries assessed by Korniyenko [89].

Table 15
Optimized set of CECs for the Nb-V-Zr system.

Phase	Parameters (J/mol)
bcc phase	e3NbVZr1 = e3NbVZr2 = e3NbVZr3 = 0. e4NbVZr1 = 0 e4NbVZr2 = 0. e4NbVZr3 = 0

parameters for the R-K polynomial are given in (34), and corresponding CECs in the CV basis are shown in Table 13. Fig. 15 presents an isothermal section calculated using these parameters. It includes the equilibrium regions for bcc and hcp phases at the Ti corner. Notably, the calculations for hcp employed the CECs from its binary subsystems without incorporating ternary interactions. The figure includes experimental data from the ternary system reported by Kornilov and Vlasov (1959) and experimental data from the Nb-Ti and Nb-V binary subsystems. Discrepancies are evident between the experimental data of Kornilov and Vlasov [78] and the experimental data used for the binary systems. We have placed greater reliance on the data of the binary subsystems and as a result the calculated phase boundaries in Fig. 15 deviate slightly from the experimental data of the ternary system.

$$\begin{aligned} L1NbTiV &= -11200, \\ L2NbTiV &= -84400, \\ L3NbTiV &= -84400 \end{aligned} \tag{34}$$

3.2.2. Nb-Ti-Zr system

Isothermal sections of the Nb-Ti-Zr ternary system have been reported by several authors over the entire composition range [84–86]. The liquidus surface and the solidus surface projections have also been investigated over the whole composition range. These studies indicated that the bcc miscibility gap in the Nb-Zr binary system extended into the ternary system and that no ternary compound formed. Equilibrium phase relationships in the Nb-Ti-Zr system were computed by Kumar et al. [68] using the Calphad approach. This work was based on thermodynamic descriptions of the binary subsystems, and ternary interactions were not considered. Later, Tokunaga et al. [86] used the same description in their Nb-Ni-Ti-Zr database. Marker et al. [87] also concluded that the interpolation of the isothermal section could reproduce the experimental phase equilibria.

Doi et al. [84] reported miscibility gap data. We have used their miscibility gap data to optimize corresponding CEC parameters. For the Nb-Zr system, miscibility gap data reported by Flewitt [88] is generally accepted and used in many assessments [61]. At 1173 K, Flewitt reported compositions of Nb-rich and Zr-rich phases as 0.24 and 0.57 at.% Zr respectively. The present binary assessment of the Nb-Zr system is also based on this data, and calculated values are 0.227 and 0.60 at % Zr. Corresponding values estimated by Doi et al. [84] are 0.22 and 0.57. Hence, the compositions of the binary Nb-rich and Zr-rich phases agree within experimental error. Since ternary interactions are likely to be weaker for this system, we have introduced minimum number of such parameters with relatively small values. Optimized parameters for the R-K polynomial are given in (35), and corresponding CECs in the CV basis are shown in Table 14. The isothermal section calculated using these parameters is shown in Fig. 16.

Table 16
Optimized set of CECs for the Ti-V-Zr system.

Phase	Parameters (J/mol)
bcc phase	e3TiVZr1 = e3TiVZrv2 = e3TiVZrr3 = 10000. e4TiVZr1 = 0 e4TiVZr2 = 0. e4TiVZr3 = 0

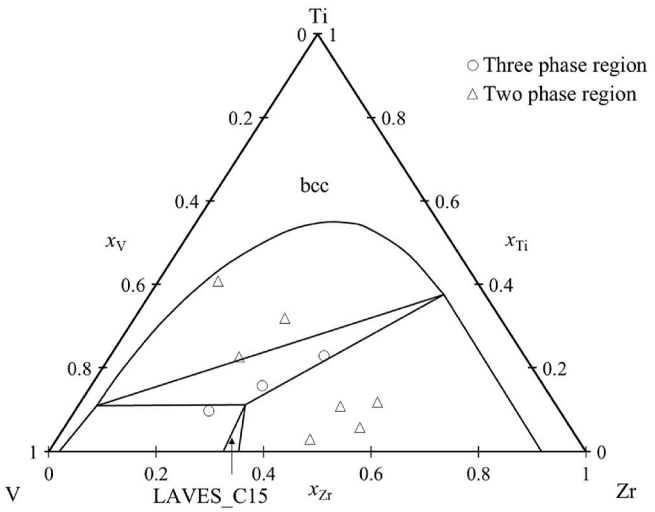

Fig. 18. Calculated isothermal section of Ti-V-Zr system at 1273 K along with experimental data of Cui et al. [70].

Table 17
CECs for the Nb-Ti-V-Zr system in the CVCF basis.

$e2NbTi1 = 6240$, $e2NbTi2 = 3120$, $e3NbTi = 0$, $e4NbTi = 0$
$e2NbV1 = 14080$, $e2NbV2 = 7040$, $e3NbV = 0$, $e4NbV = 0$,
$e2NbZr1 = 7401.6 + 6.6432T$, $e2NbZr2 = 3700.8 + 3.3216T$, $e3NbZr = -4224$, $e4NbZr = 0$
$e2TiV1 = 8160$, $e2TiV2 = 4080$, $e3TiV = 0$, $e4TiV = 0$
$e2TiZr1 = -9264$, $e2TiZr2 = -4632$, $e3TiZr = 0$, $e4TiZr = 0$
$e2VZr1 = 17920. + 2.544T$, $e2VZr2 = 8960. + 1.272T$, $e3VZr = -5760$, $e4VZr = 0$
e3NbTiV1 = e3NbTiV2 = e3NbTiV3 = − 20000. e4NbTiV1 = −48800 , e4NbTiV2 = −24400. , e4NbTiV3 = − 24400
e3NbTiZr1 = e3NbTiZr2 = e3NbTiZr3 = − 3333.33. e4NbTiZr1 = 0 e4NbTiZr2 = 0. e4NbTiZr3 = 0
e3NbVZr1 = e3NbVZr2 = e3NbVZr3 = 0. e4NbVZr1 = 0 e4NbVZr2 = 0. e4NbVZr3 = 0
e3TiVZr1 = e3TiVZrv2 = e3TiVZrr3 = 10000. e4TiVZr1 = 0 e4TiVZr2 = 0. e4TiVZr3 = 0
$e4NbTiVZr1 = e4NbTiVZr2 = e4NbTiVZr3 = 0$

$$L1NbTiZr = -10000,\quad L2NbTiZr = -10000,\quad L3NbTiZr = -10000 \tag{35}$$

3.2.3. Nb-V-Zr system

Korniyenko [89] reviewed the Nb-V-Zr System. Experimental data for this system is available in the form of liquidus and solidus surface projections, isothermal sections, and equilibria along several vertical sections. Isothermal sections drawn by Korniyenko [89] suggest the extension of the miscibility gap in the V-Zr system towards ternary compositions. Below 1073 K, the miscibility gap in the Nb-Zr system also starts extending into the ternary system. No thermodynamic assessment of this system is available in the literature. Hence LAVES_C15 phase was modeled using parameters from Ref. [90] with some modifications. Isothermal sections drawn by Korniyenko [89] show two Laves phases denoted by λ_1 and τ. However, in this work, the two phases were not distinguished, and the same model was used for both. The calculated isothermal section at 1273K is shown in Fig. 17. For this system a reasonable agreement was achieved with Korniyenko [89] without considering any ternary and quaternary interactions for the BCC phase (Table 15).

3.2.4. Ti-V-Zr system

Enomoto [91] first reviewed and assessed the Ti-V-Zr System based on experimental isothermal section data [92]. Later Cui et al. [70] obtained self-consistent thermodynamic parameters of the Ti–V–Zr system using their isothermal sections at 1073 and 1273 K and liquidus surface projection data. Ternary CECs were obtained using experimental data of Cui et al. [70] for this system. Optimized parameters for the R-K polynomial are given in (36), and corresponding CECs in the CV basis are shown in Table 16. The isothermal section calculated using these parameters is shown in Fig. 18.

$$L1TiVZr = 30000,\quad L2TiVZr = 30000,\quad L3TiVZr = 30000 \tag{36}$$

3.3. Quaternary system

Very limited information about this system is available in the literature. Gorbachev et al. [90] have given the thermodynamic description of the Nb-Ti-V-Zr system as part of their Cr–Nb–Ti–V–Zr database. The disordered bcc phase included ternary interactions only for the Ti-V-Zr system [70], and no quaternary interaction terms were considered. Hence, quaternary interactions for this system were not considered due to the unavailability of any experimental data and reliable quaternary interaction parameters.

The complete set of CECs for the Nb-V-Ti-Zr system is given in Table 17. As mentioned earlier, These are obtained after transforming CECs corresponding to the orthogonal basis given earlier by following the procedure given in Appendix 4.

4. Results and discussion

4.1. Phase diagram calculations

The V-Zr system contains the Laves phase, which also extends into the ternary regions of both Nb-V-Zr and Ti-V-Zr systems. The other binary subsystems do not exhibit any intermediate phase. To investigate the impact of high entropy stabilization of the bcc phase relative to the Laves phase, isothermal sections for five quasi-ternary alloys were computed: (Nb_1Ti_0)-V-Zr, $(Nb_{0.75}Ti_{0.25})$-V-Zr, $(Nb_{0.5}Ti_{0.5})$-V-Zr, $(Nb_{0.25}Ti_{0.75})$-V-Zr, and (Nb_0Ti_1)-V-Zr (Fig. 19). The results show significant single bcc phase stabilization in the $(Nb_{0.75}Ti_{0.25})$-V-Zr, $(Nb_{0.5}Ti_{0.5})$-V-Zr, and $(Nb_{0.25}Ti_{0.75})$-V-Zr sections. The strongest effect is observed for the $(Nb_{0.5}Ti_{0.5})$-V-Zr section, which decreases in the

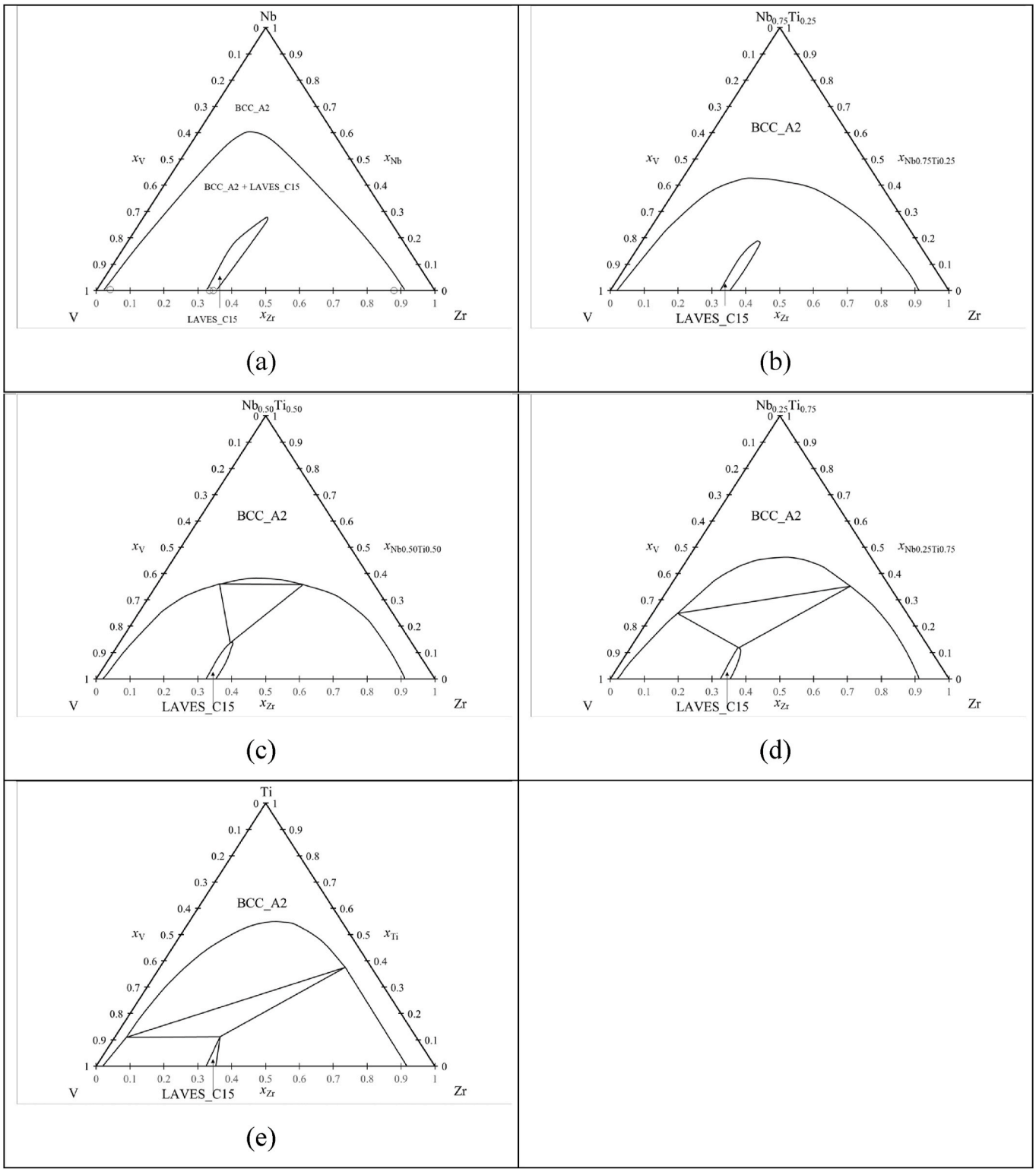

Fig. 19. Ternary and quasi-ternary isothermal section at 1273K (a) (Nb1Ti0)-V-Zr, (b) (Nb0.75Ti0.25)-V-Zr, (c) (Nb0.5Ti0.5)-V-Zr, (d) (Nb0.25Ti0.75)-V-Zr and (e) (Nb0Ti1)-V-Zr.

sections on either side of this section.

A three-phase equilibrium involving two bcc_A2 and Laves_C15 phases emerges with Nb substitution for Ti. Interestingly, this three-phase equilibrium is absent in (Nb1Ti0)-V-Zr, suggesting a dependence on the Nb/Ti ratio. This indicates that the miscibility gap in the bcc_A2 phase of the Ti-V-Zr system gradually vanishes with increasing Nb substitution.

4.2. Thermodynamic calculations

Contour plots of (a) configurational entropy, (b) enthalpy, and (c) Gibbs energy of mixing at 1273K are shown in Fig. 20. It needs to be pointed out that these calculations are relevant within the stability range of the single-phase bcc region. The miscibility gap region is marked by the dotted line in the figure. In some cases, additional phases are stable

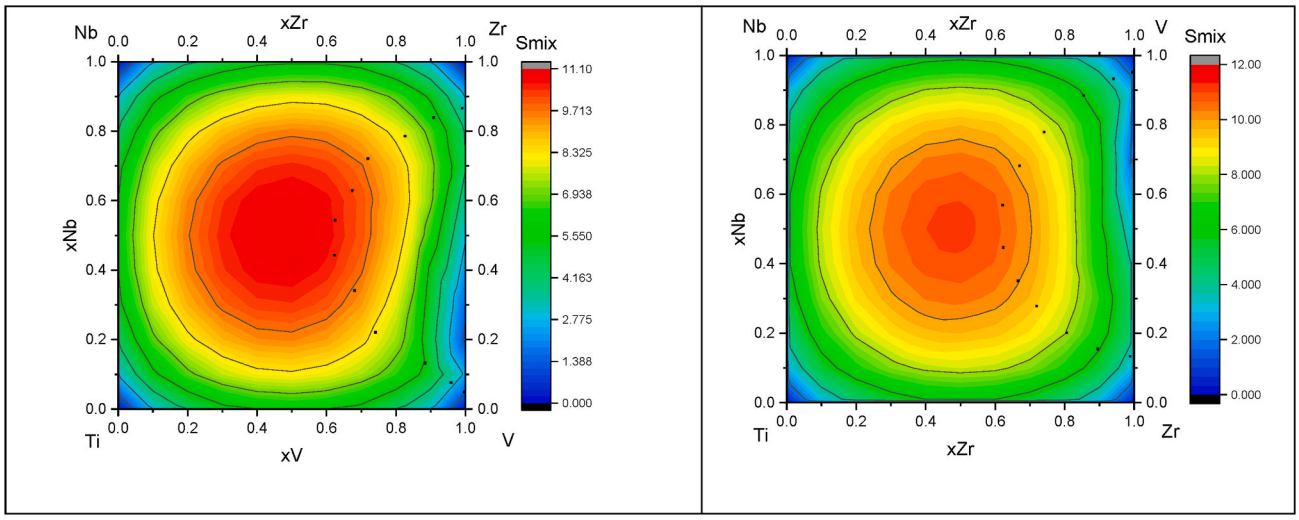

(a)

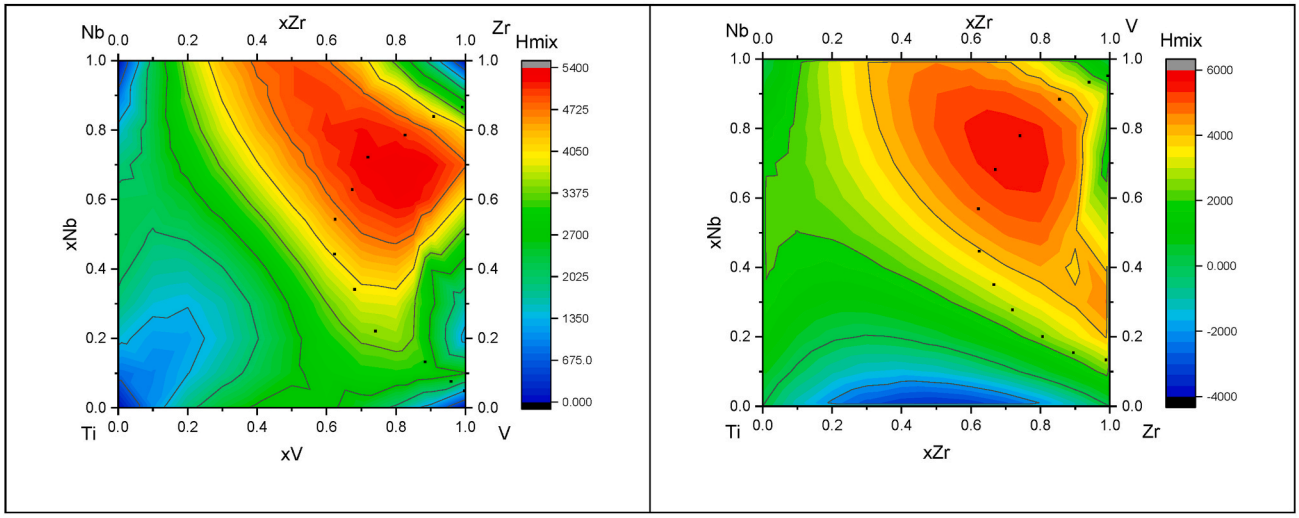

(b)

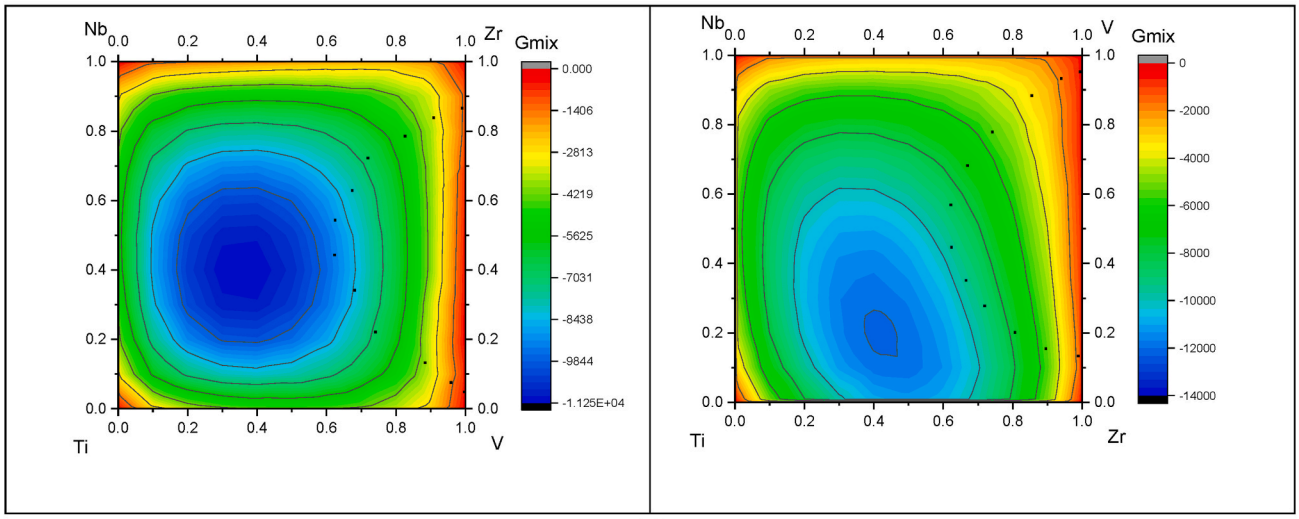

(c)

Fig. 20. Contour plots of (a) configurational entropy, (b) enthalpy, and (c) Gibbs energy of mixing at 1273K. This figure visualizes the compositions of quaternary alloys within a two-dimensional space. The dotted lines in these figures represent the boundaries of the miscibility gap. The region to the right of these lines corresponds to a two-phase region.

within this region. The results shown in the figure would be applicable to this region also if the bcc phase can be retained metastably in it. This figure visualizes the compositions of quaternary alloys within a two-dimensional space. To achieve this, calculations were performed at specific compositions where two key ratios are maintained: $x_{Ti} : x_V = x_{Nb} : x_{Zr} = (1-X)/X$ and $x_{Ti} : x_{Nb} = x_V : x_{Zr} = (1-Y)/Y$ with X and Y being the abscissa and ordinate in the plot. The composition of the alloy representing the point (X, Y) in the figure is given by

$$x_{Nb} = Y(1-X), x_{Ti} = (1-X)(1-Y), x_V = X(1-Y), x_{Zr} = XY$$

Using these two ratios, the figure effectively represents a diverse range of quaternary alloy compositions within a limited two-dimensional space. This representation has Nb-Ti, Ti-V, V-Zr, and Nb-Ti binary subsystems on the edges. To include compositions in the Ti-Zr and Nb-V systems, one more version of these contour plots is calculated with interchanged locations of V and Zr, i.e., $x_{Ti} : x_{Zr} = x_{Nb} : x_V = (1-X)/X$ and $x_{Ti} : x_{Nb} = x_{Zr} : x_V = (1-Y)/Y$.

Contour plots of the configurational entropy are almost symmetrical around equiatomic composition, except near the V-Zr end. The maximum value of entropy was 11.09 J/mol, which occurred for the alloy with the approximate composition $\{x_{Nb} = 0.27, x_{Ti} = 0.26, x_V = 0.24, x_{Zr} = 0.23\}$. The value of the entropy at the equiatomic composition was a little lower at 11.08 J/mol. These values are about 4 % lower than the ideal entropy of mixing, 11.53 J/mol.

The enthalpy of mixing reveals a tendency for phase separation in these quaternary alloys (Fig. 20b). The enthalpy is positive for all quaternary alloys, which indicates a thermodynamic preference for phase separation. This tendency is strongest in the Nb-V-Zr alloys and weakens with increasing Ti content. The maximum of the enthalpy of mixing is located near the composition $\{x_{Nb} = 0.32, x_{Ti} = 0.00, x_V = 0.34, x_{Zr} = 0.34\}$. This is in conformity with observations in binary subsystems where the bcc phase exhibits the highest phase separation tendency in the V-Zr system, followed by Nb-Zr and Nb-V. Hence, Nb-V-Zr alloys are expected to have a very high tendency for phase separation. The addition of Ti appears to counteract this tendency, suggesting a stabilization of the solid solution phase. On the other hand, the lowest value of enthalpy of mixing is located, as expected, near the equiatomic binary Ti-Zr alloy.

The combined effect of entropy and enthalpy can be observed in the Gibbs energy of mixing (Fig. 21 (c)). The minimum of the Gibbs energy is shifted toward the Ti end ($x_{Nb} = 0.115, x_{Ti} = 0.46, x_V = 0.085, x_{Zr} = 0.34$) due to the smaller contribution of the enthalpy. Iso-G contours are symmetrical around this minimum, just like in the case of entropy. Incidentally, at this composition, the entropy of mixing is just 9.60 J/mol as against the ideal value of 9.83 J mol^{-1}, and the enthalpy of mixing is almost zero. This shows the importance of enthalpy of mixing in the stabilization HEAs.

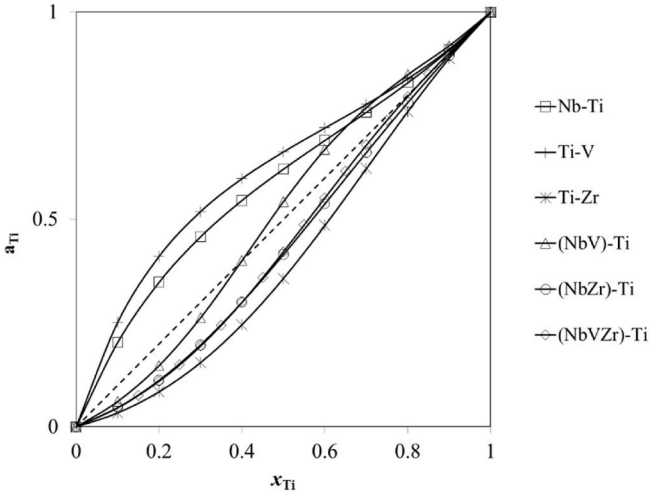

Fig. 21. Calculated activity of Ti in binary Nb-Ti, Ti-V, Ti-Zr, and pseudo-binary systems $(NbV)_xTi_{1-x}$, $(NbZr)_xTi_{1-x}$, $(NbVZr)_xTi_{1-x}$ at 1273 K.

The activity of titanium (Ti) at 1273 K was determined for binary (Nb-Ti, Ti-V, Ti-Zr), and pseudo-binary ($(NbV)_xTi_{1-x}$, $(NbZr)_xTi_{1-x}$, $(NbVZr)_xTi_{1-x}$) alloys. The results are presented in Fig. 21. As anticipated, the activity of Ti in the binary Nb-Ti and Ti-V systems deviates positively from Raoult's law. In contrast, it deviates negatively in the Ti-Zr binary solid solution. The influence of adding zirconium (Zr) on the activity of Ti in the Nb-Ti system is evident in the pseudo-binary $(NbZr)_xTi_{1-x}$ system, where a negative deviation from Raoult's law is observed. In the Nb-Ti-V system, the activity of Ti exhibits a negative departure at lower concentrations of Ti, transitioning to a positive departure at higher Ti concentrations. Interestingly, a negative deviation from Raoult's law in the quaternary alloy is observed across all compositions. These trends can be visualized more clearly in the contour maps of the activity coefficient of the Ti shown in Fig. 22. The activity coefficient of Ti in most composition regions is less than one, except near Nb- and V-rich ends, which indicates a negative departure from Raoult's law. The high phase separation tendency between Vanadium (V) and Zirconium (Zr) in the Nb-Ti-V-Zr system suggests the formation of two distinct type clusters: a V-rich region and a Zr-rich region containing Titanium (Ti). This is likely due to the attractive force between Ti and Zr, which leads to Ti co-segregating with Zr and consequently reducing its overall activity.

To understand the stabilization of quaternary bcc solutions relative to the unary, binary, and ternary counterparts, respectively, one may define the following differences for any thermodynamic quantity *F*.

$$\Delta F^{unary}(ABCD) = F(ABCD) - (1/4)(F(A) + F(B) + F(C) + F(D)) \quad (37)$$

$$\Delta F^{bin}(ABCD) = F(ABCD) - (1/6)(F(AB) + F(AC) + F(AD) + F(BC) + + A(BD) + A(CD)) \quad (38)$$

$$\Delta F^{tern}(ABCD) = F(ABCD) - (1/4)(F(ABC) + F(ABD) + F(ACD) + F(BCD)) \quad (39)$$

where *F* is any one of enthalpy, entropy, and Gibbs energy. Fig. 23 shows the variation of ΔG_{mix}, ΔH_{mix} and ΔS_{mix}. As expected, the maximum increase in entropy occurs for mixing from pure components which decreases rapidly for mixing from binary and ternary subsystems. This is accompanied by a surprising decrease in the corresponding enthalpy values. As a result, maximum stabilization is obtained with respect to pure components. However, considerable stabilization may be seen relative to ternary subsystems as well. Bokas et al. [93] have studied, using statistical analysis, the evolution of enthalpic and entropic contributions with the number of components in bcc and fcc solutions. The present results are in conformity with their conclusion that, generally, both contributions favour stabilization and that their effect decreases as the number of components increases.

4.3. SRO calculations

Pairwise multicomponent Cowley-Warren SRO parameters are defined in terms of the pair probability p_{ij}^{PR} of having P and R atoms on sites *i* and *j* [94].

$$\alpha_{PR}^{ij} = 1 - \left(\frac{p_{ij}^{PR}}{x_P x_R}\right) \quad (40)$$

Generalized pairwise multicomponent SRO parameters have been defined by Ceguerra et al. [95]. In general, one may define multisite SRO parameters (such as triangle and tetrahedron clusters) by extending the above definition as follows [96]:

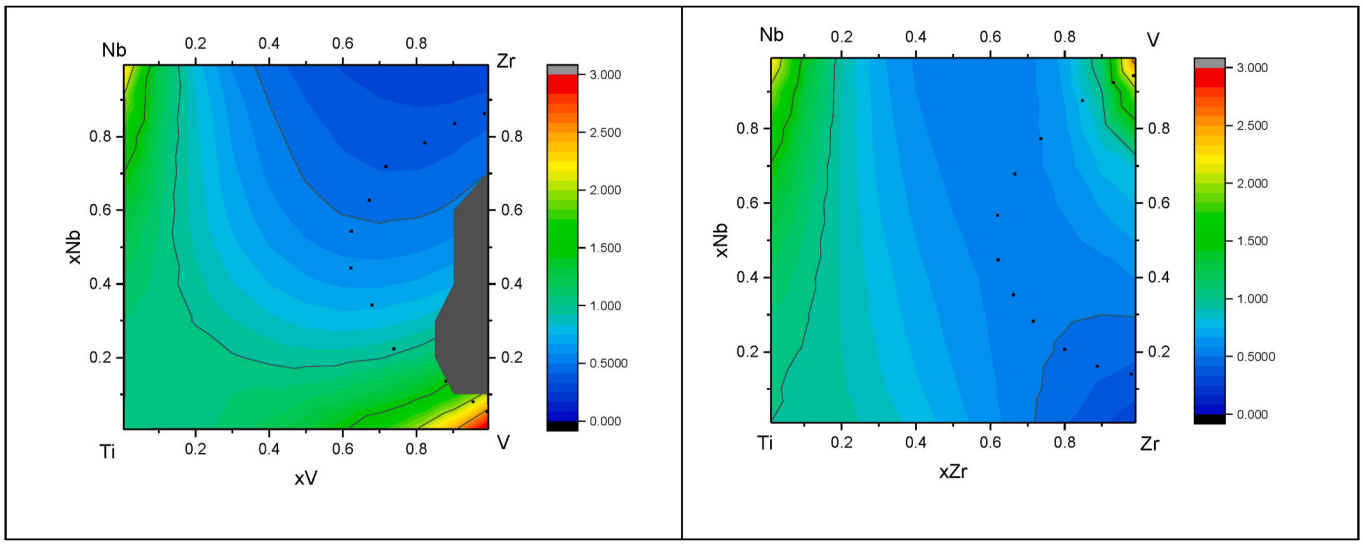

Fig. 22. Contour maps of activity coefficients of Ti calculated at 1273K

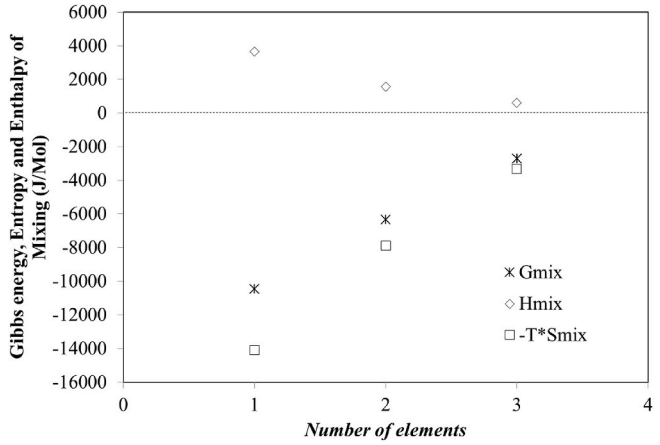

Fig. 23. Change of Gibbs energy, enthalpy, and entropy of mixing of equiatomic NbTiVZr relative to unary, binary, and ternary alloys of their components.

$$\alpha_{MPRT}^{1234} = 1 - \left(\frac{\rho_{1234}^{MPRT}}{x_M x_P x_R x_T}\right) \tag{41}$$

where ρ_{1234}^{MPRT} is the probability of having M, P, R, and T atoms on sites 1, 2, 3, and 4.

One of the advantages of the CE-CVM model is the possibility of computing the above SRO parameters, which can provide further insight into the atomic interactions. This is demonstrated through the calculation of the Cowley-Warren SRO parameters. The present formulation provides values of some of the CVs (those treated as CFs) during Gibbs energy minimization eliminating the need for additional calculations for computing SRO parameters.

The effect of composition on various first-neighbor Cowley-Warren SRO parameters (α) is shown in Fig. 24. Contour plots of Cowley–Warren first neighbor (a) Nb-Ti (b) Nb-V (c) Nb-Zr (d) Ti-V (e) Ti-Zr and (f) V-Zr pair sro parameters in pseudo-ternary isothermal section are shown in Fig. 24. These contour plots, resembling ternary diagrams, were generated by setting the mole fractions of niobium (Nb) and titanium (Ti) equal ($x_{Nb} = x_{Ti}$) while independently varying the concentrations of the remaining two alloying elements, vanadium (V) and zirconium (Zr). In the binary Nb-Ti system, a weak preference for phase separation exists, as indicated by a slightly positive SRO parameter. Adding Vanadium (V) promotes an ordering tendency, while Zirconium (Zr) enhances a phase separation tendency (Fig. 24a). This interplay continues in the quaternary system, where V and Zr create an "averaging effect," leading to a more random atomic distribution compared to the binary Nb-Ti alloy. Similarly, the Nb-Zr system exhibits a strong preference for phase separation (Fig. 24c), as reflected by its positive SRO parameter. Adding Ti intensifies this behavior while V counters it. Again, the addition of both elements results in an "averaging effect." This behavior extends to other systems. In the Ti-V system (Fig. 24d), Zr strengthens an existing phase separation tendency while Nb weakens it. The V-Zr system exhibits a strong separation tendency (Fig. 24f), reflected by its positive SRO parameter. Nb weakens this tendency, while Ti initially reduces it but leads to increased separation at higher concentrations. The binary Nb-V system exhibits a tendency for phase separation but adding Ti and Zr suppresses this and instead promotes an ordering tendency (Fig. 24b). The Ti-Zr system shows weak ordering tendencies, which are further strengthened by adding Nb and V. A combination of all the components promotes random behavior. Overall, these trends suggest that Nb-Ti-V-Zr alloys will likely form clusters enriched in V and Zr. Additionally, Nb and V might prefer to be near each other, while Ti tends to stay close to Zr.

Tetrahedron cluster sro parameters ($\alpha_{NbVTiZr}^{1234}$) based on the correlation function ($v4NbVTiZr1$) are shown in Fig. 25. One can see that this cluster at equiatomic composition has a slight phase-separating tendency. Moving toward Nb and V increases the stability of this cluster. On the other hand, the cluster becomes unstable closer to Ti and Zr. A band of instability is visible between Nb-V and Ti-Zr binary solutions. Hence, this SRO will transform into phase separation of two bcc phases at lower temperatures: (i) Nb-V rich and (ii) Ti-Zr rich. At 573 K (300 °C), equiatomic alloy separates into two phases: (i) V-rich phase ($x_{Nb} = 0.3416, x_{Ti} = 0.2389, x_V = \mathbf{0.4174}, x_{Zr} = \mathbf{0.0021}$) and (ii) Zr-rich phase ($x_{Nb} = 0.1443, x_{Ti} = 0.2656, x_V = \mathbf{0.0065}, x_{Zr} = \mathbf{0.5836}$). Nb atoms have preferential segregation with V.

The presence of SRO in single phase alloys leads to coherency strain fields which result in additional strengthening of alloys. Such strengthening is limited either by phase separation into two phases with the same crystal structure or by the formation of an ordered phase. Dasari et al. [97] have used enthalpies of mixing of binary CoFeNiAlTi alloys to infer the qualitative extent of SRO in the binary subsystems of these alloys and thereby design alloys with superior mechanical properties. The present approach shows that a quantitative mapping of SRO in the entire composition space can be achieved, and thus, compositions corresponding to desired levels of SRO can be found without elaborate

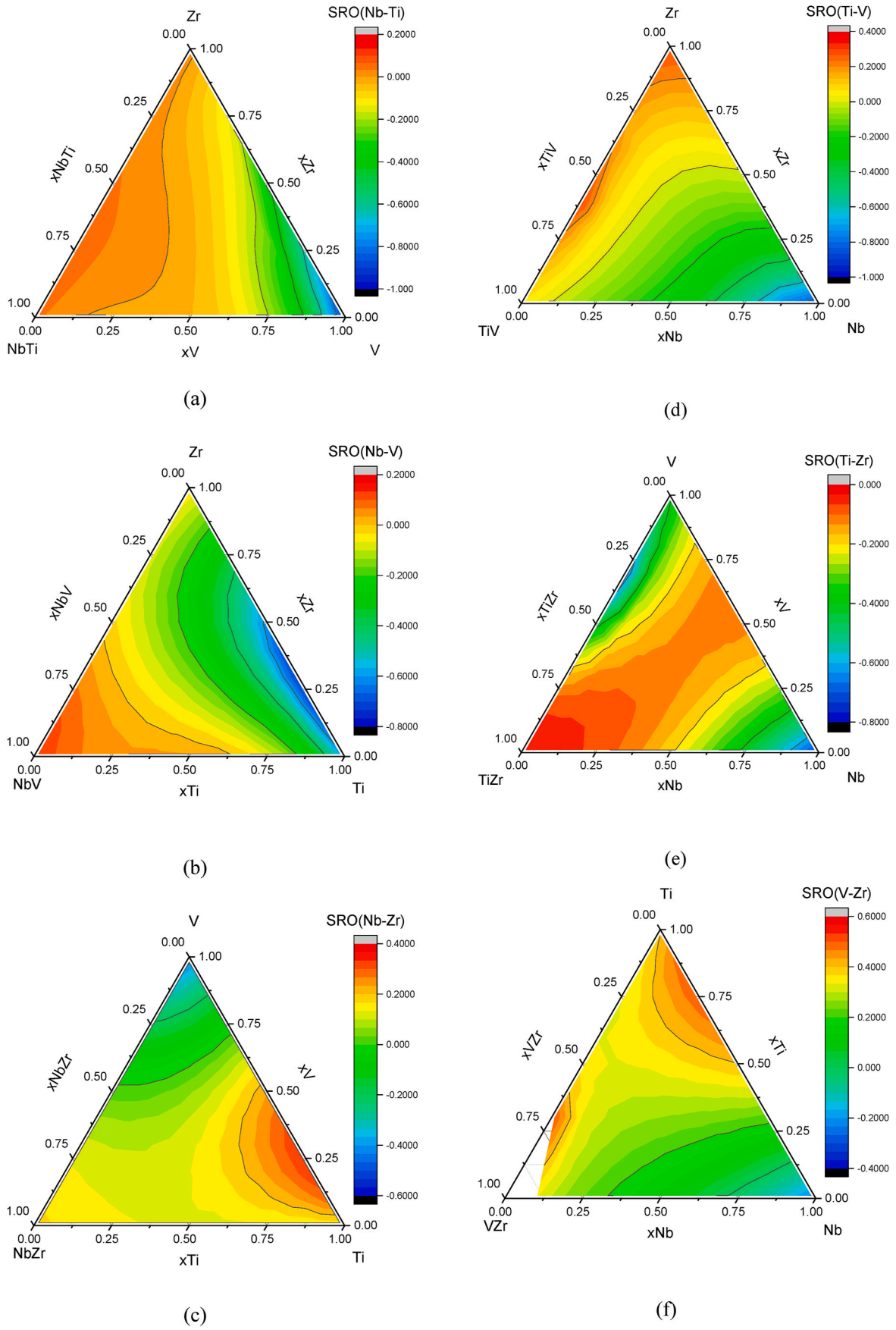

Fig. 24. Contour plots of Cowley–Warren first neighbor (a) Nb-Ti (b) Nb-V (c) Nb-Zr (d) Ti-V (e) Ti-Zr and (f) V-Zr pair sro parameters at 1273K in pseudo-ternary isothermal section of Nb-Ti-V-Zr.

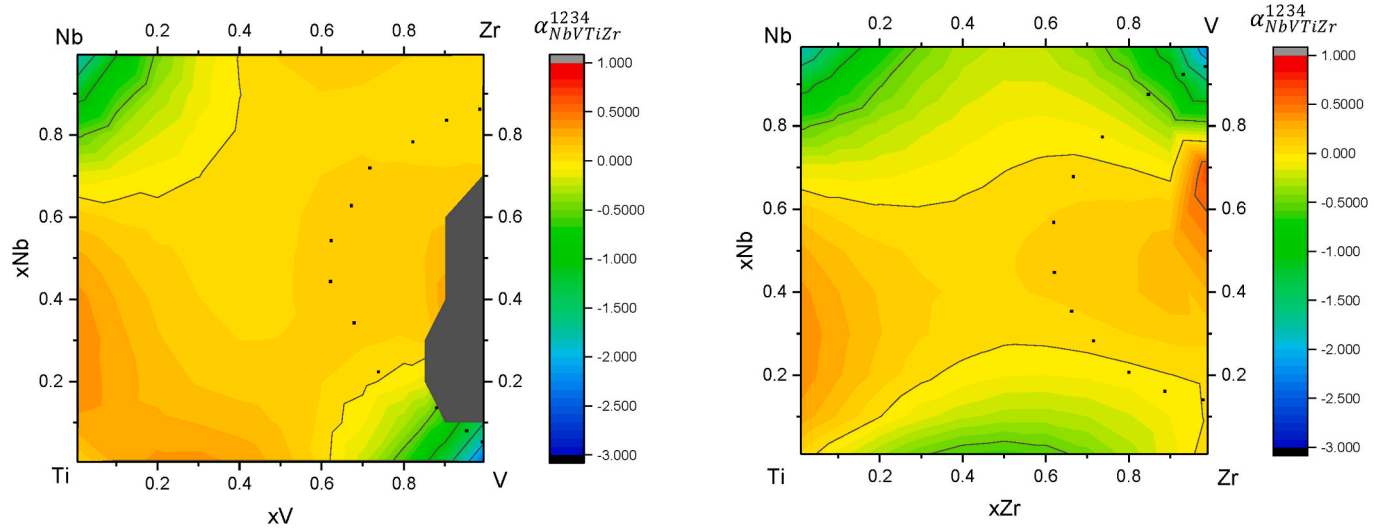

Fig. 25. Contour plots of Cowley–Warren Nb-Ti-V-Zr tetrahedron sro parameter at 1273K.

experimental investigations. In addition to pairwise SRO parameters, multisite SRO parameters can be determined to aid in alloy design. Limiting compositions corresponding to the highest values of SRO before the onset of spinodal decomposition or spinodal ordering can also be determined. Such limiting compositions should possess very high strengths.

5. Conclusions

This work introduces a novel formalism for calculating cluster expansions (CEs) used in the computational thermodynamics of multicomponent systems, which offers a consistent definition of correlation functions (CFs) across both the full system and its individual subsystems. This approach has a key advantage: the cluster expansion coefficients (CECs) of all subsystems can be directly incorporated into the CE of any higher-order system.

The details of the derivation for the multicomponent CE based on cluster variables are provided for the disordered bcc structure, while results obtained for fcc and hcp structures by a similar analysis are also presented. Notably, the CE for quinary and higher-order systems does not require any additional CECs beyond those of their constituent quaternary subsystems. This leads to two significant implications:

(i) Contrary to common belief, the number of CFs and CECs does not increase exponentially for typical multicomponent alloys.
(ii) Existing databases, like those used in standard CALPHAD methods, can be readily adapted for this CE-CVM approach.

The advantages of this formalism are demonstrated using the Nb-Ti-V-Zr system as a case study. First, thermodynamic descriptions of the binary and ternary subsystems are obtained using all available experimental data. Then, by leveraging the CECs of these subsystems, an optimized set of CECs is derived for the entire Nb-Ti-V-Zr system. Finally, various phase diagrams, thermodynamic properties and SRO parameters are calculated using this optimized set of CECs. It is shown that both enthalpy and entropy play significant roles in the stabilization of the single-phase bcc phase. Further, the low values of the Gibbs energy of mixing of the bcc phase around the equiatomic composition (owing to a favorable combination of the enthalpy and entropy of mixing) limit the range of stability of the binary Laves phase in the quaternary alloys.

CRediT authorship contribution statement

Vikas Jindal: Writing – original draft, Resources, Methodology, Investigation, Formal analysis, Data curation. **Shrikant Lele:** Writing – review & editing, Validation, Supervision, Methodology, Data curation, Conceptualization.

Declaration of competing interest

The authors declare that they have no known competing financial interests or personal relationships that could have appeared to influence the work reported in this paper.

Appendix A. Supplementary data

Supplementary data to this article can be found online at https://doi.org/10.1016/j.calphad.2025.102825.

Appendix 1. *Correlation functions for disordered fcc structure in tetrahedron approximation of CVM*

The crystallographically distinct clusters in this approximation are (sites in parenthesis): (i) Point (1), (ii) I-n pair (12), (iv) equilateral triangle (123), and (vii) Tetrahedron (1234). Details of these clusters and corresponding CFs are shown in Table 18.

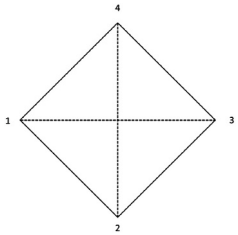

Fig. 26. Projection of tetrahedron cluster in the fcc disordered structure.

The binary system has one point, one pair, one triangle, and one tetrahedron CFs. We shall use the point variables *xA* directly as CFs along with the normalization condition $\sum xA = = 1$. there are 2 points, three pairs, four triangles, and five tetrahedra CFs for a ternary system. Out of these 14 CFs, the three binary pair CFs, three binary triangle CFs, and three binary tetrahedron CFs are directly inherited from the three binary subsystems. That leaves one ternary triangle CF and two ternary tetrahedra CFs. There are three types of triangle CVs, namely (i) ρ_{123}^{PPP}, (ii) ρ_{123}^{PPR}, ρ_{123}^{PRR} and (iii) ρ_{123}^{PRT}. Three symmetrical combinations of triangle CVs of the type ρ_{123}^{PRT} and tetrahedron CVs of the type ρ_{1234}^{PPRT}, ρ_{1234}^{PRRT}, ρ_{1234}^{PRTT} are chosen as triangle-tetrahedron composite CFs. For a quaternary system, there are 3 points, six pairs, ten triangles, and 15 tetrahedron CFs. Among these CFs, the six binary pair CFs, six binary triangle CFs, and six binary tetrahedra CFs are directly inherited from the six binary subsystems. Similarly, 4 ternary triangle and 8 ternary tetrahedron CFs are directly inherited from the 4 ternary subsystems. That leaves 1 quaternary tetrahedron CF to be defined.

Table 18
CFs for using Tetrahedron approximation for fcc structure.

System	Binary		Ternary		Quaternary	
Cluster Type	CF	No. of CF	CF	No. of CF	CF	No. of CF
Tetrahedron (1234)	*v*4 *PR*	1	*v*4 *PR*, …	3	*v*4 *PR*, …	6
			*v*4*PRT*1	1	*v*4*PRT*1, …	4
			*v*4*PRT*2	1	*v*4*PRT*2, …	4
			*v*4*PRT*3	1	*v*4*PRT*3, …	4
					*v*4*PRTW*	1
Triangle (123)	*v*3 *PR*	1	*v*3 *PR*, …	*3*	*v*3 *PR*, …	*6*
I-n Pair (12)	*v*2 *PR*	1	*v*2 *PR*, …	*3*	*v*2 *PR*, …	*6*
Point (1)	*xP*	1	*xP*, …	*2*	*xP*, …	*3*
Total no. of CFs		4		14		34

Equations (59)–(78) give expressions of CF in terms of cluster variables. CVs ρ_{12}^{PR}, ρ_{123}^{PRT}, and ρ_{1234}^{PRTW} represent probability of finding configurations *PR*, *PRT*, *PRTW* on I-n pair (12), triangle (123) and Tetrahedron (1234), respectively.

$$v2\ PR = \rho_{12}^{PR} \tag{42}$$

$$v3\ PR = \rho_{123}^{PRR} - \rho_{123}^{PPR} \tag{43}$$

$$v4PRT1 = \left(\rho_{123}^{PRT} + 2\rho_{1234}^{PPRT} - \rho_{1234}^{PRRT} - \rho_{1234}^{PRTT}\right) / 3 \tag{44}$$

$$v4PRT2 = \left(\rho_{123}^{PRT} - \rho_{1234}^{PPRT} + 2\rho_{1234}^{PRRT} - \rho_{1234}^{PRTT}\right) / 3 \tag{45}$$

$$v4PRT3 = \left(\rho_{123}^{PRT} - \rho_{1234}^{PPRT} - \rho_{1234}^{PRRT} + 2\rho_{1234}^{PRTT}\right) / 3 \tag{46}$$

$$v4\ PR = \rho_{1234}^{PPRR} \tag{47}$$

$$v4PRTW = \rho_{1234}^{PRTW} \tag{48}$$

The cluster variables' expressions for the above CFs are given below.

$$\rho_{123}^{PRT} = (v4PRT1 + v4PRT2 + v4PRT3) \tag{49}$$

$$\rho_{123}^{PPR} = \frac{1}{2}\left[(v2\ PR - v3\ PR) - \sum_{N=A}^{P-1}(v4NPR1 + v4NPR2 + v4NPR3) - \sum_{Q=P+1}^{R-1}(v4PQR1 + v4PQR2 + v4PQR3) - \sum_{S=R+1}^{Z}(v4PRS1 + v4PRS2 + v4PRS3)\right] \tag{50}$$

$$\rho_{123}^{PRR} = \frac{1}{2}\left[(v2\ PR + v3\ PR) - \sum_{N=A}^{P-1}(v4NPR1 + v4NPR2 + v4NPR3) - \sum_{Q=P+1}^{R-1}(v4PQR1 + v4PQR2 + v4PQR3) - \sum_{S=R+1}^{Z}(v4PRS1 + v4PRS2 + v4PRS3)\right] \tag{51}$$

$$\rho_{123}^{PPP} = x_P - \frac{1}{2}\sum_{M=A}^{P-1}(3v2MP + v3MP) - \frac{1}{2}\sum_{R=P+1}^{Z}(3v2\ PR - v3\ PR) + \sum_{M=A}^{P-2}\sum_{N=M+1}^{P-1}(v4MNP1 + v4MNP2 + v4MNP3) + \sum_{N=A}^{P-1}\sum_{S=P+1}^{Z}(v4NPS1 + v4NPS2 + v4NPS3) + \sum_{S=P+1}^{Z-1}\sum_{T=S+1}^{Z}(v4PST1 + v4PST2 + v4PST3) \tag{52}$$

$$\rho_{1234}^{PPRT} = v4PRT1 - \frac{1}{3}\left(\sum_{M=1}^{P-1}\rho_{1234}^{MPRT} + \sum_{Q=P+1}^{R-1}\rho_{1234}^{PQRT} + \sum_{S=R+1}^{T-1}\rho_{1234}^{PRST} + \sum_{U=T+1}^{Z}\rho_{1234}^{PRTU}\right) \tag{53}$$

$$\rho_{1234}^{PRRT} = v4PRT2 - \frac{1}{3}\left(\sum_{M=1}^{P-1}\rho_{1234}^{MPRT} + \sum_{Q=P+1}^{R-1}\rho_{1234}^{PQRT} + \sum_{S=R+1}^{T-1}\rho_{1234}^{PRST} + \sum_{U=T+1}^{Z}\rho_{1234}^{PRTU}\right) \tag{54}$$

$$\rho_{1234}^{PRTT} = v4PRT3 - \frac{1}{3}\left(\sum_{M=1}^{P-1}\rho_{1234}^{MPRT} + \sum_{Q=P+1}^{R-1}\rho_{1234}^{PQRT} + \sum_{S=R+1}^{T-1}\rho_{1234}^{PRST} + \sum_{U=T+1}^{Z}\rho_{1234}^{PRTU}\right) \tag{55}$$

$$\begin{aligned}\rho_{1234}^{PPPS} = {} & \frac{1}{2}(v2PS - v3PS - 2v4PS) - \frac{1}{2}\sum_{M=A}^{P-1}(v4MPS1 + 3v4MPS2 + v4MPS3) - \frac{1}{2}\sum_{Q=P+1}^{S-1}(3v4PQS1 + v4PQS2 + v4PQS3) \\ & - \frac{1}{2}\sum_{T=S+1}^{Z}(3v4PST1 + v4PST2 + v4PST3) + \frac{2}{3}\left(\sum_{M=A}^{P-2}\sum_{N=M+1}^{P-1}v4MNPS + \sum_{M=A}^{P-1}\sum_{Q=P+1}^{S-1}v4MPQS + \sum_{M=A}^{P-1}\sum_{T=S+1}^{Z}v4MPST\right. \\ & \left. + \sum_{Q=P+1}^{S-2}\sum_{R=Q+1}^{S-1}v4PQRS + \sum_{Q=A}^{P-1}\sum_{T=S+1}^{Z}v4PQST + \sum_{T=S+1}^{Z-1}\sum_{U=T+1}^{Z}v4PSTU\right)\end{aligned} \tag{56}$$

$$\begin{aligned}\rho_{1234}^{PSSS} = {} & \frac{1}{2}(v2PS + v3PS - 2v4PS) - \frac{1}{2}\sum_{M=A}^{P-1}(v4MPS1 + v4MPS2 + 3v4MPS3) - \frac{1}{2}\sum_{Q=P+1}^{R-1}(v4PQS1 + v4PQS2 + 3v4PQS3) \\ & - \frac{1}{2}\sum_{T=S+1}^{Z}(v4PST1 + 3v4PST2 + v4PST3) + \frac{2}{3}\left(\sum_{M=A}^{P-2}\sum_{N=M+1}^{P-1}v4MNPS + \sum_{M=A}^{P-1}\sum_{Q=P+1}^{S-1}v4MPQS + \sum_{M=A}^{P-1}\sum_{T=S+1}^{Z}v4MPST\right. \\ & \left. + \sum_{Q=P+1}^{S-2}\sum_{R=Q+1}^{S-1}v4PQRS + \sum_{Q=A}^{P-1}\sum_{T=S+1}^{Z}v4PQST + \sum_{T=S+1}^{Z-1}\sum_{U=T+1}^{Z}v4PSTU\right)\end{aligned} \tag{57}$$

$$\begin{aligned}\rho_{1234}^{PPPP} = {} & x_P - \sum_{M=A}^{P-1}(2v2MP + v3MP - v4MP) - \sum_{S=P+1}^{Z}(2v2PS - v3PS - v4PS) + 2\sum_{M=A}^{P-2}\sum_{N=M+1}^{P-1}(v4MNP1 + v4MNP2 + 2v4MNP3) \\ & + 2\sum_{N=A}^{P-1}\sum_{S=P+1}^{Z}(v4NPS1 + 2v4NPS2 + v4NPS3) + 2\sum_{S=P+1}^{Z-1}\sum_{T=S+1}^{Z}(2v4PST1 + v4PST2 + v4PST3) - 2\left(\sum_{I=A}^{P-3}\sum_{K=I+1}^{P-2}\sum_{M=K+1}^{P-1}v4IKMP\right. \\ & \left. + \sum_{K=A}^{P-2}\sum_{M=K+1}^{P-1}\sum_{R=P+1}^{Z}v4KMPR + \sum_{M=A}^{P-1}\sum_{R=P+1}^{Z-1}\sum_{T=R+1}^{Z}v4MPRT + \sum_{R=P+1}^{Z-2}\sum_{T=R+1}^{Z-1}\sum_{W=T+1}^{Z}v4PRTW\right)\end{aligned} \tag{58}$$

Appendix 2. *Correlation functions for disordered hcp structure in triangle-tetrahedron approximation of CVM*

The crystallographically distinct clusters in this approximation are (sites in parenthesis): (i) Point (1), (ii) In-plane I-n pair (12), (iii) Out-of-plane I-n pair (14), (iv) Tetrahedral basal equilateral triangle (123), (v) Octahedral basal equilateral triangle (456), (vi) Out-of-plane pyramidal isosceles triangle (124) and (vii) Tetrahedron (1234). Details of these clusters and corresponding CFs are shown in Table 19.

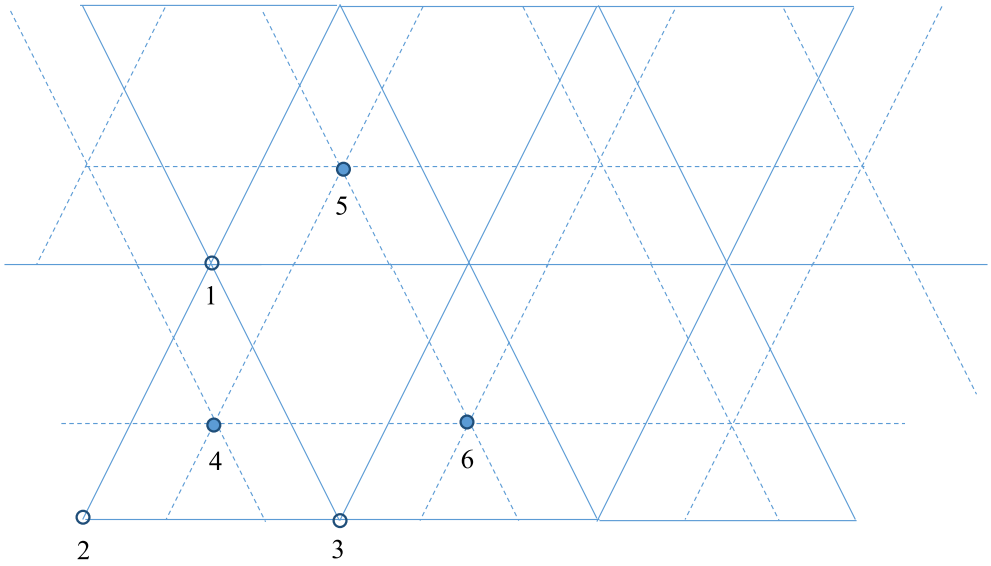

Fig. 27. Basal plane projection of hcp structure. Continuous lines connect sites on the plane of the paper, and broken lines connect the ones above and below the plane of the paper.

There is 1 point, two pairs (one in-plane and one out-of-plane), three triangles (one tetrahedral basal, one octahedral basal, and one out-of-plane),

and one tetrahedron CF in the binary system. We shall use the point variables *xA* directly as CFs along with the normalization condition $\sum xA = = 1$. Similarly, for a ternary system, there are 2 points, six pairs (three in-plane and three out-of-plane), 14 triangles (four tetrahedral basal, four octahedral basal, and six out-of-plane), and eight tetrahedra CFs. Among these 30 CFs, the six binary pair CFs, nine binary triangle CFs, and three binary tetrahedra CFs are directly inherited from the three binary subsystems. That leaves five (one tetrahedral basal, one octahedral basal, and three out-of-plane) ternary triangle CFs and five ternary tetrahedra CFs to be defined. For a quaternary system, there are 3 points, 12 pairs (six in-plane and six out-of-plane), 38 triangles (ten tetrahedral basal, ten octahedral basal, and eighteen out-of-plane), and 30 tetrahedra CFs. Out of total 83 CFs, the 12 binary pair CFs, 18 binary triangle CFs, and six binary tetrahedra CFs are directly inherited from the six binary subsystems. Similarly, 20 ternary triangles and 20 ternary tetrahedra CFs are directly inherited from the four ternary subsystems. That leaves four quaternary tetrahedra CFs to be defined.

Table 19
CFs for using Triangle-Tetrahedron approximation for cph structure.

System	Binary		Ternary		Quaternary	
Cluster Type	CF	No. of CF	CF	No. of CF	CF	No. of CF
Tetrahedron (1234)	*v4 PR*	1	*v4 PR, …*	3	*v4 PR, …*	6
			*v4PRT*31	1	*v4PRT*31, …	4
			*v4PRT*32	1	*v4PRT*32, …	4
			*v4PRT*33	1	*v4PRT*33, …	4
			*v4PRT*34	1	*v4PRT*34, …	4
			*v4PRT*35	1	*v4PRT*35, …	4
			*v4PRT*36	1	*v4PRT*36, …	4
			*v4PRT*37	1	*v4PRT*37, …	4
			*v4PRT*38	1	*v4PRT*38, …	4
			*v4PRT*39	1	*v4PRT*39, …	4
					*v4PRTW*1	1
					*v4PRTW*2	1
					*v4PRTW*3	1
					*v4PRTW*4	1
Equilateral triangle (OP) (124)	*v3 PR* 3	1	*v3 PR* 3, …	*3*	*v3 PR* 3, …	*6*
Equilateral triangle (OB) (456)	*v3 PR* 2	1	*v3 PR* 2, …	*3*	*v3PQ2,* …	*6*
			*v3PRT*2	*1*	*v3PRT2,* …	*4*
Equilateral triangle (TB) (123)	*v3 PR* 1	1	*v3 PR* 1, …	*3*	*v3 PR* 1, …	*6*
I-n Pair (OP) (14)	*v2 PR* 2	1	*v2 PR* 2, …	*3*	*v2 PR* 2, …	*6*
I-n Pair (IP) (12)	*v2 PR* 1	1	*v2 PR* 1, …	*3*	*v2 PR* 1, …	*6*
Point (1)	*xP*	1	*xP, …*	*2*	*xP, …*	*3*
Total no. of CFs		7		30		83

Equations (59)–(78) give expressions of CF in terms of cluster variables. CVs *yPR*1 and *yPR*2 represent probability of finding configuration *PR* on in-plane (12) and out-of-plane (14) pairs, respectively. Similarly, *yPRT*1, *yPRT*2 and *yPRT*3 represent probability of finding configuration *PRT* on tetrahedral basal triangle (123), octahedral basal triangle (456) and out-of-plane triangle (124), respectively. Finally, *yRTWP* is probability of finding configuration *RTWP* on the Tetrahedron (1234).

$$v2\ PR\ 1 = yPR1 \tag{59}$$

$$v2\ PR\ 2 = yPR2 \tag{60}$$

$$v3\ PR\ 1 = yPRR1 - yPPR1 \tag{61}$$

$$v3\ PR\ 2 = yPRR2 - yPPR2 \tag{62}$$

$$v3\ PR\ 3 = yRRP3 - yPPR3 \tag{63}$$

$$v4\ PR = \frac{1}{2}(yPRRP + yPPRR) \tag{64}$$

$$v3PRT2 = yPRT2 \tag{65}$$

$$v4PRT31 = yPRTP + \frac{1}{3}(yRTP3 - yPRTP - yRRTP - yRTTP) \tag{66}$$

$$v4PRT32 = yRRTP + \frac{1}{3}(yRTP3 - yPRTP - yRRTP - yRTTP) \tag{67}$$

$$v4PRT33 = yRTTP + \frac{1}{3}(yRTP3 - yPRTP - yRRTP - yRTTP) \tag{68}$$

$$v4PRT34 = yPPTR + \frac{1}{3}(yPTR3 - yPPTR - yPRTR - yPTTR) \tag{69}$$

$$v4PRT35 = yPRTR + \frac{1}{3}(yPTR3 - yPPTR - yPRTR - yPTTR) \tag{70}$$

$$v4PRT36 = yPTTR + \frac{1}{3}(yPTR3 - yPPTR - yPRTR - yPTTR) \tag{71}$$

$$v4PRT37 = yPPRT + \frac{1}{3}(yPRT3 - yPPRT - yPRRT - yPRTT) \tag{72}$$

$$v4PRT38 = yPRRT + \frac{1}{3}(yPRT3 - yPPRT - yPRRT - yPRTT) \tag{73}$$

$$v4PRT39 = yPRTT + \frac{1}{3}(yPRT3 - yPPRT - yPRRT - yPRTT) \tag{74}$$

$$v4PRTW1 = yRTWP \tag{75}$$

$$v4PRTW2 = yPTWR \tag{76}$$

$$v4PRTW1 = yPRWT \tag{77}$$

$$v4PRTW1 = yPRTW \tag{78}$$

The cluster variables' expressions for the above CFs are given below.

$$yPR1 = v2\ PR\ 1 \tag{79}$$

$$yPP1 = xP - \sum_{N=A}^{P-1} yNP1 - \sum_{Q=P+1}^{Z} yPQ1 \tag{80}$$

$$yPR2 = v2\ PR\ 2 \tag{81}$$

$$yPP2 = xP - \sum_{N=A}^{P-1} yNP2 - \sum_{Q=P+1}^{Z} yPQ2 \tag{82}$$

$$yPRT2 = v3PRT2 \tag{83}$$

$$yPPR2 = \frac{1}{2}\left(v2\ PR\ 1 - v3\ PR\ 2 - \sum_{N=A}^{P-1} v3NPR2 - \sum_{Q=P+1}^{R-1} v3PQR2 - \sum_{S=R+1}^{Z} v3PRT2\right) \tag{84}$$

$$yPRR2 = \frac{1}{2}\left(v2\ PR\ 1 + v3\ PR\ 2 - \sum_{N=A}^{P-1} v3NPR2 - \sum_{Q=P+1}^{R-1} v3PQR2 - \sum_{S=R+1}^{Z} v3PRT2\right) \tag{85}$$

$$yPPP2 = xP - \frac{3}{2}\left(\sum_{N=A}^{P-1} v2NP1 + \sum_{Q=P+1}^{Z} v2PQ1\right) + \frac{1}{2}\left(-\sum_{N=A}^{P-1} v2NP2 + \sum_{Q=P+1}^{Z} v2PQ2\right) + \sum_{L=A}^{P-2}\sum_{N=L+1}^{P-1} v3LNP2 + \sum_{N=A}^{P-1}\sum_{Q=P+1}^{Z} v3NPQ2 + \sum_{Q=P+1}^{Z-1}\sum_{S=Q+1}^{Z} v3PQS2 \tag{86}$$

$$yRTP3 = v4PRT31 + v4PRT32 + v4PRT33 \tag{87}$$

$$yPTR3 = v4PRT34 + v4PRT35 + v4PRT36 \tag{88}$$

$$yPRT3 = v4PRT37 + v4PRT38 + v4PRT39 \tag{89}$$

$$yPRTP = v4PRT31 - \frac{1}{3}\left(\sum_{N=A}^{P-1} v4NPRT2 + \sum_{Q=P+1}^{R-1} v4PQRT1 + \sum_{S=R+1}^{T-1} v4PRST1 + \sum_{U=T+1}^{Z} v4PRTU1\right) \tag{90}$$

$$yRRTP = v4PRT32 - \frac{1}{3}\left(\sum_{N=A}^{P-1} v4NPRT2 + \sum_{Q=P+1}^{R-1} v4PQRT1 + \sum_{S=R+1}^{T-1} v4PRST1 + \sum_{U=T+1}^{Z} v4PRTU1\right) \tag{91}$$

$$yRTTP = v4PRT33 - \frac{1}{3}\left(\sum_{N=A}^{P-1} v4NPRT2 + \sum_{Q=P+1}^{R-1} v4PQRT1 + \sum_{S=R+1}^{T-1} v4PRST1 + \sum_{U=T+1}^{Z} v4PRTU1\right) \tag{92}$$

$$yPPTR = v4PRT34 - \frac{1}{3}\left(\sum_{N=A}^{P-1} v4NPRT3 + \sum_{Q=P+1}^{R-1} v4PQRT3 + \sum_{S=R+1}^{T-1} v4PRST2 + \sum_{U=T+1}^{Z} v4PRTU2\right) \tag{93}$$

$$yPRTR = v4PRT35 - \frac{1}{3}\left(\sum_{N=A}^{P-1} v4NPRT3 + \sum_{Q=P+1}^{R-1} v4PQRT3 + \sum_{S=R+1}^{T-1} v4PRST2 + \sum_{U=T+1}^{Z} v4PRTU2\right) \tag{94}$$

$$yPTTR = v4PRT36 - \frac{1}{3}\left(\sum_{N=A}^{P-1} v4NPRT3 + \sum_{Q=P+1}^{R-1} v4PQRT3 + \sum_{S=R+1}^{T-1} v4PRST2 + \sum_{U=T+1}^{Z} v4PRTU2\right) \tag{95}$$

$$yPPRT = v4PRT37 - \frac{1}{3}\left(\sum_{N=A}^{P-1} v4NPRT4 + \sum_{Q=P+1}^{R-1} v4PQRT4 + \sum_{S=R+1}^{T-1} v4PRST4 + \sum_{U=T+1}^{Z} v4PRTU3\right) \tag{96}$$

$$yPRRT = v4PRT38 - \frac{1}{3}\left(\sum_{N=A}^{P-1} v4NPRT4 + \sum_{Q=P+1}^{R-1} v4PQRT4 + \sum_{S=R+1}^{T-1} v4PRST4 + \sum_{U=T+1}^{Z} v4PRTU3\right) \tag{97}$$

$$yPRTT = v4PRT39 - \frac{1}{3}\left(\sum_{N=A}^{P-1} v4NPRT4 + \sum_{Q=P+1}^{R-1} v4PQRT4 + \sum_{S=R+1}^{T-1} v4PRST4 + \sum_{U=T+1}^{Z} v4PRTU3\right) \tag{98}$$

$$\begin{aligned} yPPR3 = \frac{1}{2}\Bigg[& -v2\,PR\,1 + 2v2\,PR\,2 - v3\,PR\,3 - \sum_{M=A}^{P-1}(-v4MPR31 - v4MPR32 - v4MPR33 + v4MPR34 + v4MPR35 + v4MPR36 + v4MPR37 \\ & + v4MPR38 + v4MPR39) - \sum_{Q=P+1}^{R-1}(v4PQR31 + v4PQR32 + v4PQR33 - v4PQR34 - v4PQR35 - v4PQR36 + v4PQR37 + v4PQR38 \\ & + v4PQR39) - \sum_{S=R+1}^{Z}(v4PRS31 + v4PRS32 + v4PRS33 + v4PRS34 + v4PRS35 + v4PRS36 - v4PRS37 - v4PRS38 - v4PRS39)\Bigg] \end{aligned} \tag{99}$$

$$\begin{aligned} yRRP3 = \frac{1}{2}\Bigg[& -v2\,PR\,1 + 2v2\,PR\,2 + v3\,PR\,3 - \sum_{M=A}^{P-1}(-v4MPR31 - v4MPR32 - v4MPR33 + v4MPR34 + v4MPR35 + v4MPR36 + v4MPR37 \\ & + v4MPR38 + v4MPR39) - \sum_{Q=P+1}^{R-1}(v4PQR31 + v4PQR32 + v4PQR33 - v4PQR34 - v4PQR35 - v4PQR36 + v4PQR37 + v4PQR38 \\ & + v4PQR39) - \sum_{S=R+1}^{Z}(v4PRS31 + v4PRS32 + v4PRS33 + v4PRS34 + v4PRS35 + v4PRS36 - v4PRS37 - v4PRS38 - v4PRS39)\Bigg] \end{aligned} \tag{100}$$

$$\begin{aligned} yPRR3 = \frac{1}{2}\Bigg[& v2\,PR\,1 + v3\,PR\,3 + \sum_{M=A}^{P-1}(-v4MPR31 - v4MPR32 - v4MPR33 + v4MPR34 + v4MPR35 + v4MPR36 - v4MPR37 - v4MPR38 \\ & - v4MPR39) + \sum_{Q=P+1}^{R-1}(v4PQR31 + v4PQR32 + v4PQR33 - v4PQR34 - v4PQR35 - v4PQR36 - v4PQR37 - v4PQR38 - v4PQR39) \\ & + \sum_{S=R+1}^{Z}(v4PRS31 + v4PRS32 + v4PRS33 - v4PRS34 - v4PRS35 - v4PRS36 - v4PRS37 - v4PRS38 - v4PRS39)\Bigg] \end{aligned} \tag{101}$$

$$\begin{aligned} yPRP3 = \frac{1}{2}\Bigg[& v2\,PR\,1 - v3\,PR\,3 + \sum_{M=A}^{P-1}(-v4MPR31 - v4MPR32 - v4MPR33 + v4MPR34 + v4MPR35 + v4MPR36 - v4MPR37 - v4MPR38 \\ & - v4MPR39) + \sum_{Q=P+1}^{R-1}(v4PQR31 + v4PQR32 + v4PQR33 - v4PQR34 - v4PQR35 - v4PQR36 - v4PQR37 - v4PQR38 - v4PQR39) \\ & + \sum_{S=R+1}^{Z}(v4PRS31 + v4PRS32 + v4PRS33 - v4PRS34 - v4PRS35 - v4PRS36 - v4PRS37 - v4PRS38 - v4PRS39)\Bigg] \end{aligned} \tag{102}$$

$$\begin{aligned} yPPP3 = {} & xP - \frac{1}{2}\sum_{M=A}^{P-1}(v2MP1 + 2v2MP2 - v3MP3) - \frac{1}{2}\sum_{M=A}^{P-1}(v2\,PR\,1 + 2v2\,PR\,2 + v3\,PR\,3) + \sum_{M=A}^{P-2}\sum_{N=M+1}^{P-1}(v4MNP37 + v4MNP38 + v4MNP39) \\ & + \sum_{M=A}^{P-1}\sum_{R=P+1}^{Z}(v4MPR34 + v4MPR35 + v4MPR36) + \sum_{Q=P+1}^{Z-1}\sum_{R=Q+1}^{Z}(v4PQR31 + v4PQR32 + v4PQR33) \end{aligned} \tag{103}$$

$$\begin{aligned} yPRT1 = {} & v4PRT31 + v4PRT35 + v4PRT39 + \frac{1}{3}\Bigg[\sum_{N=A}^{P-1}(3v4NPRT1 - v4NPRT2 - v4NPRT3 - v4NPRT4) + \sum_{Q=P+1}^{R-1}(3v4PQRT2 - v4PQRT1 \\ & - v4PQRT3 - v4PQRT4) + \sum_{S=R+1}^{T-1}(3v4PRST3 - v4PRST1 - v4PRST2 - v4PRST4) + \sum_{U=T+1}^{Z}(3v4PRTU4 - v4PRTU1 - v4PRTU2 \\ & - v4PRTU3)\Bigg] \end{aligned} \tag{104}$$

$$\begin{aligned} yPPT1 = \frac{1}{2}\Bigg[& v2PT1 - v3PT1 - \sum_{N=A}^{P-1}(v4NPT31 + v4NPT35 + v4NPT39) - \sum_{Q=P+1}^{T-1}(v4PQT31 + v4PQT35 + v4PQT39) \\ & - \sum_{U=T+1}^{Z}(v4PTU31 + v4PRU35 + v4PRU39)\Bigg] + \frac{1}{3}\Bigg[\sum_{L=A}^{P-2}\sum_{N=L+1}^{P-1}(-v4LNPT1 - v4LNPT2 + v4LNPT3 + v4LNPT4) \\ & + \sum_{N=A}^{P-1}\sum_{Q=P+1}^{R-1}(-v4NPQT1 + v4NPQT2 - v4NPQT3 + v4NPQT4) + \sum_{N=A}^{P-1}\sum_{U=T+1}^{Z}(-v4NPTU1 + v4NPTU2 + v4NPTU3 - v4NPTU4) \\ & + \sum_{Q=P+1}^{T-2}\sum_{R=Q+1}^{T-1}(v4PQRT1 - v4PQRT2 - v4PQRT3 + v4PQRT4) + \sum_{Q=P+1}^{T-1}\sum_{U=T+1}^{Z}(v4PQTU1 - v4PQTU2 + v4PQTU3 - v4PQTU4) \\ & + \sum_{U=T+1}^{Z-1}\sum_{V=U+1}^{Z}(v4PTUV1 + v4PTUV2 - v4PTUV3 - v4PTUV4)\Bigg] \end{aligned} \tag{105}$$

$$yPTT1 = \frac{1}{2}\Bigg[v2PT1 - v3PT1 - \sum_{N=A}^{P-1}(v4NPT31 + v4NPT35 + v4NPT39) - \sum_{Q=P+1}^{T-1}(v4PQT31 + v4PQT35 + v4PQT39) - \sum_{U=T+1}^{Z}(v4PTU31 + v4PRU35 + v4PRU39)\Bigg] + \frac{1}{3}\Bigg[\sum_{L=A}^{P-2}\sum_{N=L+1}^{P-1}(-v4LNPT1 - v4LNPT2 + v4LNPT3 + v4LNPT4) + \sum_{N=A}^{P-1}\sum_{Q=P+1}^{R-1}(-v4NPQT1 + v4NPQT2 - v4NPQT3 + v4NPQT4) + \sum_{N=A}^{P-1}\sum_{U=T+1}^{Z}(-v4NPTU1 + v4NPTU2 + v4NPTU3 - v4NPTU4) + \sum_{Q=P+1}^{T-2}\sum_{R=Q+1}^{T-1}(v4PQRT1 - v4PQRT2 - v4PQRT3 + v4PQRT4) + \sum_{Q=P+1}^{T-1}\sum_{U=T+1}^{Z}(v4PQTU1 - v4PQTU2 + v4PQTU3 - v4PQTU4) + \sum_{U=T+1}^{Z-1}\sum_{V=U+1}^{Z}(v4PTUV1 + v4PTUV2 - v4PTUV3 - v4PTUV4)\Bigg] \tag{106}$$

$$yPPP1 = xP - \frac{3}{2}\left(\sum_{N=A}^{P-1}v2NP1 + \sum_{R=P+1}^{Z}v2\ PR\ 1\right) + \frac{1}{2}\left(-\sum_{N=A}^{P-1}v3NP1 + \sum_{R=P+1}^{Z}v3\ PR\ 1\right) + \sum_{M=A}^{P-2}\sum_{N=M+1}^{P-1}(v4MNP31 + v4MNP35 + v4MNP39) + \sum_{N=A}^{P-1}\sum_{R=P+1}^{Z}(v4NPR31 + v4NPR35 + v4NPR39) + \sum_{R=P+1}^{Z-1}\sum_{T=R+1}^{Z}(v4PRT31 + v4PRT35 + v4PRT39) + \frac{1}{3}\Bigg[\sum_{L=A}^{P-3}\sum_{M=L+1}^{P-2}\sum_{N=M+1}^{P-1}(v4LMNP1 + v4LMNP2 + v4LMNP3 - 3v4LMNP4) + \sum_{M=A}^{P-2}\sum_{N=M+1}^{P-1}\sum_{Q=P+1}^{Z}(v4MNPQ1 + v4MNPQ2 - 3v4MNPQ3 + v4LMNP4) + \sum_{N=A}^{P-1}\sum_{Q=P+1}^{Z-1}\sum_{R=Q+1}^{Z}(v4NPQR1 - 3v4NPQR2 + v4NPQR3 + v4NPQR4) + \sum_{Q=P+1}^{Z-2}\sum_{R=Q+1}^{Z-1}\sum_{S=R+1}^{Z}(-3v4PQRS1 + v4PQRS2 + v4PQRS3 + v4PQRS4)\Bigg] \tag{107}$$

$$yPPTP = \frac{1}{4}(2\ v2PT1 - v3PT1 - v3PT3 - 4\ v4PT) + \frac{1}{4}\sum_{L=A}^{P-1}(-2\ v4LPT31 - 3\ v4LPT32 - v4LPT33 - v4LPT34 - 4\ v4LPT35 - v4LPT36 + v4LPT37 + v4LPT38) + \frac{1}{4}\sum_{Q=P+1}^{T-1}(-4\ v4PQT31 - v4PQT32 - v4PQT33 - 3\ v4PQT34 - 2\ v4PQT35 - v4PQT36 + v4PQT37 + v4PQT38) + \frac{1}{4}\sum_{U=T+1}^{Z}(-4\ v4PTU31 - v4PTU32 - v4PTU33 + v4PTU34 + v4PTU36 - 3\ v4PTU37 - v4PTU38 - 2\ v4PTU39) + \frac{1}{6}\sum_{L=A}^{P-2}\sum_{M=L+1}^{P-1}(3\ v4LMPT3 + v4LMPT4) + \frac{1}{6}\sum_{L=A}^{P-1}\sum_{Q=P+1}^{T-1}(3\ v4LMPT2 + v4LMPT4) + +\frac{1}{6}\sum_{L=A}^{P-1}\sum_{U=T+1}^{Z}(3\ v4LPTU2 + v4LPTU3) + \frac{1}{6}\sum_{Q=P+1}^{T-2}\sum_{R=Q+1}^{T-1}(3\ v4PQRT1 + v4PQRT4) + \frac{1}{6}\sum_{Q=P+1}^{T-1}\sum_{U=T+1}^{Z}(3\ v4PQTU1 + v4PQTU3) + \frac{1}{6}\sum_{U=T+1}^{Z-1}\sum_{W=U+1}^{Z}(3\ v4PTUW1 + v4PTUW2) \tag{108}$$

$$yPTTT = \frac{1}{4}(2\ v2PT1 + v3PT1 + v3PT3 - 4\ v4PT) + \frac{1}{4}\sum_{L=A}^{P-1}(-2\ v4LPT31 - v4LPT32 - 3\ v4LPT33 + v4LPT34 + v4LPT36 - v4LPT37 - v4LPT38 - 4\ v4LPT39) + \frac{1}{4}\sum_{Q=P+1}^{T-1}(v4PQT32 + v4PQT33 - v4PQT34 - 2\ v4PQT35 - 3\ v4PQT36 - v4PQT37 - v4PQT38 - 4\ v4PQT39) + \frac{1}{4}\sum_{U=T+1}^{Z}(v4PTU32 + v4PTU33 - v4PTU34 - 4\ v4PTU35 - v4PTU36 - v4PTU37 - 3\ v4PTU38 - 2\ v4PTU39) + \frac{1}{6}\sum_{L=A}^{P-2}\sum_{M=L+1}^{P-1}(v4LMPT3 + 3\ v4LMPT4) + \frac{1}{6}\sum_{L=A}^{P-1}\sum_{Q=P+1}^{T-1}(v4LMPT2 + 3\ v4LMPT4) + +\frac{1}{6}\sum_{L=A}^{P-1}\sum_{U=T+1}^{Z}(v4LPTU2 + 3\ v4LPTU3) + \frac{1}{6}\sum_{Q=P+1}^{T-2}\sum_{R=Q+1}^{T-1}(v4PQRT1 + 3\ v4PQRT4) + \frac{1}{6}\sum_{Q=P+1}^{T-1}\sum_{U=T+1}^{Z}(v4PQTU1 + 3\ v4PQTU3) + \frac{1}{6}\sum_{U=T+1}^{Z-1}\sum_{W=U+1}^{Z}(v4PTUW1 + 3\ v4PTUW2) \tag{109}$$

$$yPPTT = \frac{1}{4}(-v3PT1 + v3PT3 + 4\ v4PT) + \frac{1}{4}\sum_{L=A}^{P-1}(-v4LPT32 + v4LPT33 + v4LPT34 + 2\ v4LPT35 + v4LPT36 - v4LPT37 - v4LPT38 - 2\ v4LPT39) + \frac{1}{4}\sum_{Q=P+1}^{T-1}(2\ v4PQT31 + v4PQT32 + v4PQT33 - v4PQT34 + v4PQT36 - v4PQT37 - v4PQT38 - 2\ v4PQT39) + \frac{1}{4}\sum_{U=T+1}^{Z}(2\ v4PTU31 + v4PTU32 + v4PTU33 - v4PTU34 - 2\ v4PTU35 - v4PTU36 - v4PTU37 + v4PTU38) + \frac{1}{6}\sum_{L=A}^{P-2}\sum_{M=L+1}^{P-1}(-v4LMPT3 + v4LMPT4) + \frac{1}{6}\sum_{L=A}^{P-1}\sum_{Q=P+1}^{T-1}(-v4LMPT2 + v4LMPT4) + +\frac{1}{6}\sum_{L=A}^{P-1}\sum_{U=T+1}^{Z}(-v4LPTU2 + v4LPTU3) + \frac{1}{6}\sum_{Q=P+1}^{T-2}\sum_{R=Q+1}^{T-1}(-v4PQRT1 + v4PQRT4) + \frac{1}{6}\sum_{Q=P+1}^{T-1}\sum_{U=T+1}^{Z}(-v4PQTU1 + v4PQTU3) + \frac{1}{6}\sum_{U=T+1}^{Z-1}\sum_{W=U+1}^{Z}(-v4PTUW1 + v4PTUW2) \tag{110}$$

$$yPTTP = \frac{1}{4}(v3PT1 - v3PT3 - 4\ v4PT) - \frac{1}{4}\sum_{L=A}^{P-1}(-v4LPT32 + v4LPT33 + v4LPT34 + 2\ v4LPT35 + v4LPT36 - v4LPT37 - v4LPT38 - 2\ v4LPT39)$$
$$- \frac{1}{4}\sum_{Q=P+1}^{T-1}(2\ v4PQT31 + v4PQT32 + v4PQT33 - v4PQT34 + v4PQT36 - v4PQT37 - v4PQT38 - 2\ v4PQT39)$$
$$- \frac{1}{4}\sum_{U=T+1}^{Z}(2\ v4PTU31 + v4PTU32 + v4PTU33 - v4PTU34 - 2\ v4PTU35 - v4PTU36 - v4PTU37 + v4PTU38) - \frac{1}{6}\sum_{L=A}^{P-2}\sum_{M=L+1}^{P-1}($$
$$- v4LMPT3 + v4LMPT4) - \frac{1}{6}\sum_{L=A}^{P-1}\sum_{Q=P+1}^{T-1}(-v4LMPT2 + v4LMPT4) - \frac{1}{6}\sum_{L=A}^{P-1}\sum_{U=T+1}^{Z}(-v4LPTU2 + v4LPTU3) - \frac{1}{6}\sum_{Q=P+1}^{T-2}\sum_{R=Q+1}^{T-1}($$
$$- v4PQRT1 + v4PQRT4) - \frac{1}{6}\sum_{Q=P+1}^{T-1}\sum_{U=T+1}^{Z}(-v4PQTU1 + v4PQTU3) - \frac{1}{6}\sum_{U=T+1}^{Z-1}\sum_{W=U+1}^{Z}(-v4PTUW1 + v4PTUW2) \tag{111}$$

$$yPPPT = \frac{1}{4}(-2\ v2PT1 + 4\ v2PT2 + v3PT1 - 3\ v3PT3 - 4\ v4PT)$$
$$+ \frac{1}{4}\sum_{L=A}^{P-1}(2\ v4LPT31 + 3\ v4LPT32 + v4LPT33 - 3\ v4LPT34 - 4\ v4LPT35 - 3\ v4LPT36 - v4LPT37 - 5\ v4LPT38) + \frac{1}{4}\sum_{Q=P+1}^{T-1}($$
$$- 4\ v4PQT31 - 3\ v4PQT32 - 3\ v4PQT33 + 3\ v4PQT34 + 2\ v4PQT35 + v4PQT36 - v4PQT37 - v4PQT38) + \frac{1}{4}\sum_{U=T+1}^{Z}($$
$$- 4\ v4PTU31 - 3\ v4PTU32 - 3\ v4PTU33 - 5\ v4PTU34 - v4PTU36 + 3\ v4PTU37 + v4PTU38 + 2\ v4PTU39)$$
$$+ \frac{1}{6}\sum_{L=A}^{P-2}\sum_{M=L+1}^{P-1}(v4LMPT3 + 3\ v4LMPT4) + \frac{1}{6}\sum_{L=A}^{P-1}\sum_{Q=P+1}^{T-1}(v4LMPT2 + 3\ v4LMPT4) + +\frac{1}{6}\sum_{L=A}^{P-1}\sum_{U=T+1}^{Z}(v4LPTU2 + 3\ v4LPTU3)$$
$$+ \frac{1}{6}\sum_{Q=P+1}^{T-2}\sum_{R=Q+1}^{T-1}(v4PQRT1 + 3\ v4PQRT4) + \frac{1}{6}\sum_{Q=P+1}^{T-1}\sum_{U=T+1}^{Z}(v4PQTU1 + 3\ v4PQTU3) + \frac{1}{6}\sum_{U=T+1}^{Z-1}\sum_{W=U+1}^{Z}(v4PTUW1 + 3\ v4PTUW2) \tag{112}$$

$$yTTTP = \frac{1}{4}(-2\ v2PT1 + 4\ v2PT2 - v3PT1 + 3\ v3PT3 - 4\ v4PT)$$
$$+ \frac{1}{4}\sum_{L=A}^{P-1}(2\ v4LPT31 + v4LPT32 + 3\ v4LPT33 - v4LPT34 - 5\ v4LPT36 - 3\ v4LPT37 - 3\ v4LPT38 - 4\ v4LPT39) + \frac{1}{4}\sum_{Q=P+1}^{T-1}($$
$$- v4PQT32 - 5\ v4PQT33 + v4PQT34 + 2\ v4PQT35 + 3\ v4PQT36 - 3\ v4PQT37 - 3\ v4PQT38 - 4\ v4PQT39) + \frac{1}{4}\sum_{U=T+1}^{Z}($$
$$- 5\ v4PTU32 - v4PTU33 - 3\ \ v4PTU34 - 4\ v4PTU35 - 3\ v4PTU36 + v4PTU37 + 3\ v4PTU38 + 2\ v4PTU39)$$
$$+ \frac{1}{6}\sum_{L=A}^{P-2}\sum_{M=L+1}^{P-1}(3\ v4LMPT3 + v4LMPT4) + \frac{1}{6}\sum_{L=A}^{P-1}\sum_{Q=P+1}^{T-1}(3\ v4LMPT2 + v4LMPT4) + +\frac{1}{6}\sum_{L=A}^{P-1}\sum_{U=T+1}^{Z}(3\ v4LPTU2 + v4LPTU3)$$
$$+ \frac{1}{6}\sum_{Q=P+1}^{T-2}\sum_{R=Q+1}^{T-1}(3\ v4PQRT1 + v4PQRT4) + \frac{1}{6}\sum_{Q=P+1}^{T-1}\sum_{U=T+1}^{Z}(3\ v4PQTU1 + v4PQTU3) + \frac{1}{6}\sum_{U=T+1}^{Z-1}\sum_{W=U+1}^{Z}(3\ v4PTUW1 + v4PTUW2) \tag{113}$$

$$yPPPP = xP - \sum_{L=A}^{P-1}(v2LP1 + v2LP2 - v4LP) - \sum_{U=P+1}^{Z}(v2PU1 + v2PU2 - v4PU) - \frac{1}{4}\sum_{L=A}^{P-1}(v3LP1 + 3\ v3LP3) + \frac{1}{4}\sum_{U=P+1}^{Z}(v3PU1 + 3\ v3PU3)$$
$$+ \frac{1}{2}\sum_{L=A}^{P-2}\sum_{M=L+1}^{P-1}(v4LMP31 + v4LMP33 + v4LMP35 + v4LMP36 + 3\ v4LMP37 + 3\ v4LMP38 + 6\ v4LMP39)$$
$$+ \frac{1}{2}\sum_{L=A}^{P-1}\sum_{U=P+1}^{Z}(v4LPU31 + v4LPU32 + 3\ v4LPU34 + 6\ v4LPU35 + 3\ v4LPU36 + v4LPU38 + v4LPU39)$$
$$+ \frac{1}{2}\sum_{R=P+1}^{Z-1}\sum_{U=R+1}^{Z}(6\ v4LPU31 + 3\ v4LPU32 + 3\ v4LPU33 + v4LPU34 + v4LPU35 + v4LPU37 + v4LPU39)$$
$$+ \frac{1}{6}\sum_{L=A}^{P-3}\sum_{M=L+1}^{P-2}\sum_{N=M+1}^{P-1}(v4LMNP1 + v4LMNP2 + v4LMNP3 + 9\ v4LMNP4)$$
$$+ \frac{1}{6}\sum_{L=A}^{P-2}\sum_{M=L+1}^{P-1}\sum_{U=P+1}^{Z}(v4LMNP1 + v4LMNP2 + 9\ v4LMNP3 + v4LMNP4)$$
$$+ \frac{1}{6}\sum_{L=A}^{P-1}\sum_{R=P+1}^{Z-1}\sum_{U=R+1}^{Z}(v4LMNP1 + 9\ v4LMNP2 + v4LMNP3 + v4LMNP4)$$
$$+ \frac{1}{6}\sum_{Q=P+1}^{Z-2}\sum_{R=Q+1}^{Z-1}\sum_{U=R+1}^{Z}(9\ v4LMNP1 + v4LMNP2 + v4LMNP3 + v4LMNP4) \tag{114}$$

Appendix 3. *Transformation of Redlich-Kister parameters for the disordered bcc (A2) structure to CECs in CV basis*

A simple scheme of transforming Redlich-Kister parameters for the disordered bcc (A2) structure to CECs will be shown in this section. These transformed CECs can serve a good initial value for developing multicomponent CE-CVM databases. For a binary system P-Q, Eqn. (30) reduced to

$$H_c = e21PQ \bullet v21PQ + e22PQ \bullet v22PQ + e3PQ \bullet v3PQ + e4PQ \bullet v4PQ \tag{115}$$

The above equation can be written in the random limit by replacing the average of the product of site occupation operators with the product of the averages of these operators. As an example

$$v3PQ = \langle p_1^Q \bullet p_2^P \bullet p_3^Q \rangle - \langle p_1^P \bullet p_2^Q \bullet p_3^P \rangle \rightarrow \langle p_1^Q \rangle \langle p_2^P \rangle \langle p_3^Q \rangle - \langle p_1^P \rangle \langle p_2^Q \rangle \langle p_3^P \rangle$$

$$= x_P \bullet x_Q^2 - x_P^2 \bullet x_Q = -x_P \bullet x_Q(x_P - x_Q)$$

Substituting such random values in Eqn. (30) yields

$$H_c(\text{bin, rnd}) = e21PQ \bullet x_P \bullet x_Q + e22PQ \bullet x_P \bullet x_Q - e3PQ \bullet x_P \bullet x_Q(x_P - x_Q) + e4PQ \bullet \frac{1}{4} x_P \bullet x_Q\left[1 - (x_P - x_Q)^2\right] \tag{116}$$

The above expression may be compared with the Redlich-Kister polynomial for a binary solution.

$$H_c(\text{bin}, R-K) = x_P \bullet x_Q\left[L0PQ + L1PQ(x_P - x_Q) + L2PQ(x_P - x_Q)^2\right]$$

A comparison of the above two expressions leads to the following equivalence between the Redlich-Kister parameters and the CECs in the CVCF basis:

$$\begin{aligned} L0PQ + L2PQ &= e21PQ + e22PQ \\ L1PQ &= -e3PQ \\ L2PQ &= -\frac{1}{4} e4PQ \end{aligned} \tag{117}$$

Explicit solutions for $e21PQ$ and $e22PQ$ are not possible. Similar relations hold for binary subsystems of higher-order systems.

The ternary excess enthalpy in the random limit is given by

$$H_c(\text{tern, rnd}) = x_P \bullet x_Q \bullet x_R(e3PQR1 + e3PQR2 + e3PQR3 + e4PQR1 \bullet x_P + e4PQR2 \bullet x_Q + e4PQR3 \bullet x_R) \tag{118}$$

The corresponding term in CALPHAD is usually expressed as

$$H_c(\text{tern, CALPHAD}) = \frac{1}{3} x_P \bullet x_Q \bullet x_R[L1PQR(1 + 2x_P - x_Q - x_R) + L2PQR(1 + 2x_Q - x_R - x_P) + L3PQR(1 + 2x_R - x_P - x_Q)] \tag{119}$$

Comparing the coefficients of these expressions, we get

$$\begin{aligned} (L1PQR + L2PQR + L3PQR)[1 - f(x_P + x_Q + x_R)] &= 3(e3PQR1 + e3PQR2 + e3PQR3) \\ 3L1PQR - (1-f)(L1PQR + L2PQR + L3PQR) &= 3e4PQR1 \\ 3L2PQR - (1-f)(L1PQR + L2PQR + L3PQR) &= 3e4PQR2 \\ 3L3PQR - (1-f)(L1PQR + L2PQR + L3PQR) &= 3e4PQR3 \end{aligned} \tag{120}$$

Since they are not unique, we have introduced an arbitrary parameter f in the above relations. Explicit solutions for $e3PQR1$, $e3PQR2$, and $e3PQR3$ are not possible. Similar relations hold for ternary subsystems of higher-order systems.

For $f = 0$

$$\begin{aligned} (e3PQR1 + e3PQR2 + e3PQR3) &= \frac{1}{3}(L1PQR + L2PQR + L3PQR) \\ e4PQR1 &= L1PQR - \frac{1}{3}(L1PQR + L2PQR + L3PQR) \\ e4PQR2 &= L2PQR - \frac{1}{3}(L1PQR + L2PQR + L3PQR) \\ e4PQR3 &= L3PQR - \frac{1}{3}(L1PQR + L2PQR + L3PQR) \end{aligned} \tag{121}$$

The quaternary excess enthalpy in the random limit is given by

$$H_c(\text{qtrn, rnd}) = x_P \bullet x_Q \bullet x_R \bullet x_S(e4PQRS1 + e4PQRS2 + e4PQRS3)$$

The corresponding term in CALPHAD is usually expressed as

$$H_c(q\text{trn, CALPHAD}) = x_P \bullet x_Q \bullet x_R \bullet x_S \bullet LPQRS$$

Comparing the coefficients of these expressions, we get

$$LPQRS = e4PQRS1 + e4PQRS2 + e4PQRS3 \tag{122}$$

Once again, explicit solutions for $e4PQRS1$, $e4PQRS2$, and $e4PQRS3$ are not possible. Similar relations hold for quaternary subsystems of higher-order systems. Similar expressions can be obtained for fcc and hcp structures as well.

Appendix 4. *Transformation of CECs in the orthogonal basis for the disordered bcc (A2) structure to CECs in CV basis*

For a binary system P-Q, H_c in the orthogonal basis can be written as

$$H_c^o = +4E21PQ(u21PQ - 1) + 3E22PQ(u22PQ - 1) + 12E3PQ(u3PQ + xP - xQ) + 6E4PQ(u4PQ - 1) \tag{123}$$

The above equation can be written in the random limit by replacing the average of the product of site occupation operators with the product of the averages of these operators. As an example

$$u21PQ = \langle s_1^P \bullet s_2^Q \rangle = \langle s_1^P \rangle \langle s_2^Q \rangle$$

$$= (x_Q - x_P)^2$$

Substituting such random values in Eqn. (123) yields

$$H_c^o(\text{bin},\text{rnd}) = +4E21PQ\left((x_Q - x_P)^2 - 1\right) + 3E22PQ\left((x_Q - x_P)^2 - 1\right) + 12E3PQ\left((x_Q - x_P)^3 + xP - xQ\right) + 6E4PQ\left((x_Q - x_P)^4 - 1\right)$$
$$= x_P \bullet x_Q \bullet (-16 \bullet E21PQ - 12 \bullet E22PQ + 48 \bullet E3PQ(x_P - x_Q) + 96 \bullet E4 \bullet x_P \bullet x_Q) \quad (124)$$

The above expression may be compared with a similar expression on the CVCF basis.

$$H_c(\text{bin},\text{rnd}) = x_P \bullet x_Q \bullet (e21PQ + e22PQ - e3PQ \bullet (x_P - x_Q) + e4PQ \bullet x_P \bullet x_Q)$$

A comparison of the above two expressions leads to the following equivalence between the CECs on the orthogonal basis and the CECs on the CVCF basis:

$$-16 \bullet E21PQ - 12 \bullet E22PQ = e21PQ + e22PQ$$
$$48 \bullet E3PQ = -e3PQ \quad (125)$$
$$96 \bullet E4PQ = e4PQ$$

Explicit solutions for $e21PQ$ and $e22PQ$ are not possible. Similar relations hold for binary subsystems of higher-order systems.

In a specific case where $E22PQ = \frac{2}{3}E21PQ$

$$e21PQ + e22PQ = -24 \bullet E21PQ \quad (126)$$

Data availability

The raw data supporting the symbols in the figures is provided as a supplementary file. Additional data can be made available upon reasonable request.

References

[1] J.M.M. Sanchez, F. Ducastelle, D. Gratias, Generalized cluster description of multicomponent systems, Phys. A Stat. Mech. Its Appl. 128 (1984) 334–350, https://doi.org/10.1016/0378-4371(84)90096-7.

[2] M. Asta, D. de Fontaine, M. van Schilfgaarde, M. Sluiter, M. Methfessel, First-principles phase-stability study of fcc alloys in the Ti-Al system, Phys. Rev. B 46 (1992) 5055–5072, https://doi.org/10.1103/PhysRevB.46.5055.

[3] M. Asta, S.M. Foiles, A.A. Quong, First-principles calculations of bulk and interfacial thermodynamic properties for fcc-based Al-Sc alloys, Phys. Rev. B 57 (1998) 11265–11275, https://doi.org/10.1103/PhysRevB.57.11265.

[4] V. Blum, A. Zunger, Structural complexity in binary bcc ground states: the case of bcc Mo-Ta, Phys. Rev. B 69 (2004) 020103, https://doi.org/10.1103/PhysRevB.69.020103.

[5] J.A.D. Connolly, A. Williams, Density-functional theory applied to phase transformations in transition-metal alloys, Phys. Rev. B 27 (1983) 5169–5172, https://doi.org/10.1103/PhysRevB.27.5169.

[6] S. Curtarolo, W. Setyawan, G.L.W. Hart, M. Jahnatek, R.V. Chepulskii, R.H. Taylor, S. Wang, J. Xue, K. Yang, O. Levy, M.J. Mehl, H.T. Stokes, D.O. Demchenko, D. Morgan, AFLOW: an automatic framework for high-throughput materials discovery, Comput. Mater. Sci. 58 (2012) 218–226, https://doi.org/10.1016/j.commatsci.2012.02.005.

[7] D. De Fontaine, Cluster approach to order-disorder transformations in alloys, in: Solid State Phys., 1994, pp. 33–176, https://doi.org/10.1016/S0081-1947(08)60639-6.

[8] A. Díaz-Ortiz, H. Dosch, R. Drautz, Cluster expansions in multicomponent systems: precise expansions from noisy databases, J. Phys. Condens. Matter 19 (2007) 406206, https://doi.org/10.1088/0953-8984/19/40/406206.

[9] R. Drautz, M. Fähnle, Spin-cluster expansion: parametrization of the general adiabatic magnetic energy surface with ab initio accuracy, Phys. Rev. B 69 (2004) 104404, https://doi.org/10.1103/PhysRevB.69.104404.

[10] G.D. Garbulsky, G. Ceder, Linear-programming method for obtaining effective cluster interactions in alloys from total-energy calculations: application to the fcc Pd-V system, Phys. Rev. B 51 (1995) 67–72, https://doi.org/10.1103/PhysRevB.51.67.

[11] G. Ghosh, A. van de Walle, M. Asta, First-principles calculations of the structural and thermodynamic properties of bcc, fcc and hcp solid solutions in the Al-TM (TM = Ti, Zr and Hf) systems: a comparison of cluster expansion and supercell methods, Acta Mater. 56 (2008) 3202–3221, https://doi.org/10.1016/j.actamat.2008.03.006.

[12] G.L.W. Hart, V. Blum, M.J. Walorski, A. Zunger, Evolutionary approach for determining first-principles Hamiltonians, Nat. Mater. 4 (2005) 391–394, https://doi.org/10.1038/nmat1374.

[13] D. Lerch, O. Wieckhorst, G.L.W. Hart, R.W. Forcade, S. Müller, UNCLE: a code for constructing cluster expansions for arbitrary lattices with minimal user-input, Model. Simulat. Mater. Sci. Eng. 17 (2009) 055003, https://doi.org/10.1088/0965-0393/17/5/055003.

[14] J.Z. Liu, A. van de Walle, G. Ghosh, M. Asta, Structure, energetics, and mechanical stability of Fe-Cu bcc alloys from first-principles calculations, Phys. Rev. B 72 (2005) 144109, https://doi.org/10.1103/PhysRevB.72.144109.

[15] Z.W. Lu, S.-H. Wei, A. Zunger, S. Frota-Pessoa, L.G. Ferreira, First-principles statistical mechanics of structural stability of intermetallic compounds, Phys. Rev. B 44 (1991) 512–544, https://doi.org/10.1103/PhysRevB.44.512.

[16] A.A. Mbaye, L.G. Ferreira, A. Zunger, First-principles calculation of semiconductor-alloy phase diagrams, Phys. Rev. Lett. 58 (1987) 49–52, https://doi.org/10.1103/PhysRevLett.58.49.

[17] D. Morgan, A. van de Walle, G. Ceder, J.D. Althoff, D. de Fontaine, Vibrational thermodynamics: coupling of chemical order and size effects, Model. Simulat. Mater. Sci. Eng. 8 (2000) 295–309, https://doi.org/10.1088/0965-0393/8/3/310.

[18] M.H.F. Sluiter, D. de Fontaine, X. Guo, R. Podloucky, A. Freeman, First-principles calculation of phase equilibria in the aluminum lithium system, Phys. Rev. B 42 (1990) 10460–10476, https://doi.org/10.1103/PhysRevB.42.10460.

[19] M.H.F. Sluiter, Y. Kawazoe, Cluster expansion method for adsorption: application to hydrogen chemisorption on graphene, Phys. Rev. B 68 (2003) 085410, https://doi.org/10.1103/PhysRevB.68.085410.

[20] A. Van der Ven, M.K. Aydinol, G. Ceder, G. Kresse, J. Hafner, First-principles investigation of phase stability in LixCoO2, Phys. Rev. B 58 (1998) 2975–2987, https://doi.org/10.1103/PhysRevB.58.2975.

[21] A. Van der Ven, G. Ceder, M. Asta, P.D. Tepesch, First-principles theory of ionic diffusion with nondilute carriers, Phys. Rev. B 64 (2001) 184307, https://doi.org/10.1103/PhysRevB.64.184307.

[22] Q. Wu, B. He, T. Song, J. Gao, S. Shi, Cluster expansion method and its application in computational materials science, Comput. Mater. Sci. 125 (2016) 243–254, https://doi.org/10.1016/j.commatsci.2016.08.034.

[23] J.M. Sanchez, Foundations and practical implementations of the cluster expansion, J. Phase Equilibria Diffus. 38 (2017) 238–251, https://doi.org/10.1007/s11669-017-0521-3.

[24] J.M. Sanchez, Renormalized interactions in truncated cluster expansions, Phys. Rev. B 99 (2019) 134206, https://doi.org/10.1103/PhysRevB.99.134206.

[25] G.B. Taggart, Generalized Flinn operators with applications to multi-component alloys, J. Phys. Chem. Solid. 34 (1973) 1917–1925, https://doi.org/10.1016/S0022-3697(73)80114-3.

[26] W.P.G. Inden, Atomic Ordering, Vol. 5 of Materials Science and Technology, vol. 5, VCH, Weinheim, Ger, 1991, p. 497. Chap. 9, VCH, Weinheim, Germany.

[27] B.N. Sarma, S. Lele, Transformations among CE-CVM model parameters for multicomponent systems, Bull. Mater. Sci. 28 (2005) 293–298, https://doi.org/10.1007/BF02711263.

[28] A. van de Walle, Multicomponent multisublattice alloys, nonconfigurational entropy and other additions to the Alloy Theoretic Automated Toolkit, Calphad 33 (2009) 266–278, https://doi.org/10.1016/j.calphad.2008.12.005.

[29] X. Zhang, M.H.F. Sluiter, Cluster expansions for thermodynamics and kinetics of multicomponent alloys, J. Phase Equilibria Diffus. (2015), https://doi.org/10.1007/s11669-015-0427-x.

[30] A. Fernández-Caballero, M. Fedorov, J. Wróbel, P. Mummery, D. Nguyen-Manh, Configurational entropy in multicomponent alloys: matrix formulation from ab initio based Hamiltonian and application to the FCC Cr-Fe-Mn-Ni system, Entropy 21 (2019) 68, https://doi.org/10.3390/e21010068.

[31] P. Cenedese, D. Gratias, Multicomponent formalism in the mean-field approximation: a geometric interpretation of Chebychev polynomials, Phys. A Stat. Mech. Its Appl. 179 (1991) 277–287, https://doi.org/10.1016/0378-4371(91)90065-K.

[32] J.M. Sanchez, T. Mohri, Approximate solutions to the cluster variation free energies by the variable basis cluster expansion, Comput. Mater. Sci. 122 (2016) 301–306, https://doi.org/10.1016/j.commatsci.2016.05.035.

[33] C. Wolverton, D. de Fontaine, Cluster expansions of alloy energetics in ternary intermetallics, Phys. Rev. B 49 (1994) 8627–8642, https://doi.org/10.1103/PhysRevB.49.8627.

[34] B.N. Sarma, S.N. Shah, M. Kumar, S. Lele, Thermodynamics of dilute binary solid solutions using the cluster variation method, Int. J. Mater. Res. (Formerly

Zeitschrift Fuer Met. 103 (2012) 1188–1200, https://doi.org/10.3139/146.110755.
[35] R.P. Gorrey, V. Jindal, B.N. Sarma, S. Lele, Analytical solutions for the correlation functions of perfectly ordered binary phases based on bcc, fcc and cph structures using cluster variation method, Calphad 71 (2020) 101773, https://doi.org/10.1016/j.calphad.2020.101773.
[36] O. Redlich, A.T. Kister, Algebraic representation of thermodynamic properties and the classification of solutions, Ind. Eng. Chem. 40 (1948) 345–348, https://doi.org/10.1021/ie50458a036.
[37] H.L.H. Lukas, S.G.S. Fries, B. Sundman, Computational Thermodynamics: the Calphad Method, Cambridge University Press, Cambridge, 2007.
[38] S. Lele, B.N. Sarma, Computational thermodynamics of Sc–Zr and Sc–Ti alloys using cluster variation method, J. Mater. Sci. 44 (2009) 2334–2342, https://doi.org/10.1007/s10853-008-3197-6.
[39] N. Kumar, U.V. Waghmare, Entropic stabilization and descriptors of structural transformation in high entropy alloys, Acta Mater. 255 (2023) 119077, https://doi.org/10.1016/j.actamat.2023.119077.
[40] P. Clapp, S. Moss, Correlation functions of disordered binary alloys. I, Phys. Rev. 142 (1966) 418–427, https://doi.org/10.1103/PhysRev.142.418.
[41] M.H.F. Sluiter, Y. Kawazoe, Invariance of truncated cluster expansions for first-principles alloy thermodynamics, Phys. Rev. B Condens. Matter 71 (2005) 1–2, https://doi.org/10.1103/PhysRevB.71.212201.
[42] J.M. Sanchez, Cluster expansion and the configurational theory of alloys, Phys. Rev. B 81 (2010) 224202, https://doi.org/10.1103/PhysRevB.81.224202.
[43] V. Jindal, B.N. Sarma, S. Lele, A thermodynamic assessment of the Cr–Mo system using CE-CVM, Calphad 43 (2013) 80–85, https://doi.org/10.1016/j.calphad.2013.10.003.
[44] M. Hillert, A discussion of methods of calculating phase diagrams, Bull. Alloy Phase Diag. 2 (1981) 265–268, https://doi.org/10.1007/BF02868269.
[45] M. Hillert, Some viewpoints on the use of a computer for calculating phase diagrams, Physica B+C 103 (1981) 31–40, https://doi.org/10.1016/0378-4363(81)91000-7.
[46] S. Kumar, V. Jindal, Thermodynamic Re-assessment of the Nb-Zr system using the CE–CVM model for solid solution phases, J. Phase Equilibria Diffus. 43 (2022) 277–286, https://doi.org/10.1007/s11669-022-00959-4.
[47] S. Kumar, V. Jindal, First-principles calculations and thermodynamic assessment of the Nb–V system using CE-CVM, Calphad 78 (2022) 102439, https://doi.org/10.1016/j.calphad.2022.102439.
[48] S. Kumar, V. Jindal, Modeling short-range ordering in binary BCC Ti-X (X = Nb, V, Zr) alloys using CE-CVM, J. Phase Equilibria Diffus. 43 (2022) 511–526, https://doi.org/10.1007/s11669-022-00989-y.
[49] L. Kaufman, H. Bernstein, Computer Calculation of Phase Diagrams, Academic Press, New York, 1970.
[50] J.L. Murray, The Nb−Ti (Niobium-Titanium) system, Bull. Alloy Phase Diag. 2 (1981) 55–61, https://doi.org/10.1007/BF02873704.
[51] J.L. Murray, P.K. Liao, K.E. Spear, Phase Diagrams of Binary Titanium Alloys, ASM International, Metals Park, OH, 1987.
[52] K.C.H. Kumar, P. Wollants, L. Delaey, Thermodynamic calculation of Nb-Ti-V phase diagram, Calphad 18 (1994) 71–79, https://doi.org/10.1016/0364-5916(94)90008-6.
[53] Y. Zhang, H. Liu, Z. Jin, Thermodynamic assessment of the Nb-Ti system, Calphad 25 (2001) 305–317, https://doi.org/10.1016/S0364-5916(01)00051-7.
[54] A.K. Thakur, V.K. Pandey, V. Jindal, Calculation of existence domains and optimized phase diagram for the Nb-Ti binary alloy system using computational methods, J. Phase Equilibria Diffus. 41 (2020) 846–858, https://doi.org/10.1007/s11669-020-00843-z.
[55] V.V. Molokanov, D.B. Chernov, P.B. Budberg, Calculation of the phase diagrams for the vanadium-chromium, vanadium-niobium, and chromium-niobium systems in terms of the regular solution approximation, Russ. J. Phys. Chem. 51 (1977) 1181–1183.
[56] S.S. Balakrishna, A.K. Mallik, Synthesis of azeotropic and two terminal solid solution type binary diagrams, Calphad 3 (1979) 109–118, https://doi.org/10.1016/0364-5916(79)90011-7.
[57] J.F. Smith, O.N. Carlson, The Nb−V (Niobium-Vanadium) system, Bull. Alloy Phase Diag. 4 (1983) 46–49, https://doi.org/10.1007/BF02880319.
[58] E. Rudy, Compendium of Phase Diagram Data, Air Force Materials Laboratory, Part V, 1969, pp. 110–111.
[59] J. Gao, C. Li, J. Dang, C. Guo, Z. Du, Experimental determination and thermodynamic description of the Nb-V binary system, J. Alloys Compd. 768 (2018) 316–322, https://doi.org/10.1016/j.jallcom.2018.07.254.
[60] J.P. Abriata, J.C. Bolcich, The Nb-Zr (Niobium-Zirconium) system, Bull. Alloy Phase Diag. 3 (1982) 34–44, https://doi.org/10.1007/BF02873409.
[61] A. Fernandez Guillermet, Thermodynamic analysis of the stable phases in the Zr - Nb system and calculation of the phase diagram, Zeitschrift Fuer Met. Res. Adv. Tech. 82 (1991) 478–487.
[62] P. Lafaye, C. Toffolon-Masclet, J.-C. Crivello, J.-M. Joubert, Experimental investigations and thermodynamic modelling of the Cr–Nb–Sn–Zr system, Calphad 64 (2019) 43–54, https://doi.org/10.1016/j.calphad.2018.11.002.
[63] J.L. Murray, The Ti−V (Titanium-Vanadium) system, Bull. Alloy Phase Diag. 2 (1981) 48–55, https://doi.org/10.1007/BF02873703.
[64] N. Saunders, System Ti-V, in: I. Ansara, A.T. Dinsdale, M.H. Rand (Eds.), COST 507, "Thermochemical Database Light Met. Alloy vol. 2, EUR 18499, 1998, pp. 297–298.
[65] G. Ghosh, Thermodynamic and kinetic modeling of the Cr-Ti-V system, J. Phase Equil. 23 (2002) 310–328, https://doi.org/10.1361/105497102770331569.
[66] N.V.V. Skripnyak, A.V.V. Ponomareva, M.P.P. Belov, E.A.A. Syutkin, A.V.V. Khvan, A.T.T. Dinsdale, I.A.A. Abrikosov, Mixing enthalpies of alloys with dynamical instability: bcc Ti-V system, Acta Mater. 188 (2020) 145–154, https://doi.org/10.1016/j.actamat.2020.01.056.
[67] J.L. Murray, The Ti−Zr (Titanium-Zirconium) system, Bull. Alloy Phase Diag. 2 (1981) 197–201, https://doi.org/10.1007/BF02881478.
[68] K.C. Hari Kumar, P. Wollants, L. Delacy, Thermodynamic assessment of the Ti-Zr system and calculation of the Nb-Ti-Zr phase diagram, J. Alloys Compd. 206 (1994) 121–127, https://doi.org/10.1016/0925-8388(94)90019-1.
[69] M.A. Turchanin, P.G. Agraval, A.R. Abdulov, Thermodynamic assessment of the Cu-Ti-Zr system. II. Cu-Zr and Ti-Zr systems, Powder Metall. Met. Ceram. 47 (2008) 428–446, https://doi.org/10.1007/s11106-008-9039-x.
[70] J. Cui, C. Guo, L. Zou, Changrong Li, Z. Du, Experimental investigation and thermodynamic modeling of the Ti–V–Zr system, Calphad 55 (2016) 189–198, https://doi.org/10.1016/j.calphad.2016.09.003.
[71] U. Thiedemann, M. Rosner-kuhn, K. Drewes, G. Kuppermann, M.G. Frohberg, Mixing enthalpy measurements of liquid Ti-Zr , Fe-Ti-Zr and Fe-Ni-Zr, Alloy. 70 (1999) 3–8.
[72] S. Sridar, R. Kumar, K.C.H. Kumar, Calphad : computer coupling of phase diagrams and thermodynamic modelling of Ti-Zr-N system, Calphad 56 (2017) 102–107, https://doi.org/10.1016/j.calphad.2016.12.003.
[73] J. Korb, K. Hack, System V-Zr, in: I. Ansara, A.T. Dinsdale, M.H. Rand (Eds.), COST 507, Defin. Thermochem. Thermophys. Prop. To Provid. a Database Dev. New Light Alloy, 1998, pp. 303–304. Luxembourg.
[74] C. Servant, Thermodynamic assessments of the phase diagrams of the hafnium-vanadium and vanadium-zirconium systems, J. Phase Equilibria Diffus. 26 (2005) 39–49, https://doi.org/10.1007/s11669-005-0056-x.
[75] X.-S. Zhao, G.-H. Yuan, M.-Y. Yao, Q. Yue, J.-Y. Shen, First-principles calculations and thermodynamic modeling of the V–Zr system, Calphad 36 (2012) 163–168, https://doi.org/10.1016/j.calphad.2011.07.003.
[76] J. Cui, C. Guo, L. Zou, C. Li, Z. Du, Thermodynamic modeling of the V–Zr system supported by key experiments, Calphad 53 (2016) 122–129, https://doi.org/10.1016/j.calphad.2016.03.008.
[77] J.T. Williams, Vanadium-zirconium alloy system, J. Occup. Med. 7 (1955) 345–350, https://doi.org/10.1007/BF03377505.
[78] I.I. Kornilov, V.S. Vlasov, Phase diagram of titanium- vanadium-niobium system, Russ. J. Inorg. Chem. 4 (1959) 734–738.
[79] S. Komjathy, The constitution of some vanadium-base binary and ternary systems and the ageing characteristics of selected ternary alloys, J. Less Common Met. 3 (1961) 468–488, https://doi.org/10.1016/0022-5088(61)90032-7.
[80] M. Enomoto, The Nb-Ti-V system (Niobium-Titanium-Vanadium), J. Phase Equil. 12 (1991) 359–362, https://doi.org/10.1007/BF02649927.
[81] J.Y. Lee, J.H. Kim, H.M. Lee, Effect of Mo and Nb on the phase equilibrium of the Ti–Cr–V ternary system in the non-burning β-Ti alloy region, J. Alloys Compd. 297 (2000) 231–239, https://doi.org/10.1016/S0925-8388(99)00557-5.
[82] Z. Wei, C. Wang, S. Qin, Y. Lu, X. Yu, X. Liu, Assessment of atomic mobilities for bcc phase in the Ti-Nb-V system, J. Phase Equilibria Diffus. 41 (2020) 191–206, https://doi.org/10.1007/s11669-020-00801-9.
[83] B. Hu, B. Yao, J. Wang, Y. Liu, C. Wang, Y. Du, H. Yin, The phase equilibria of the Ti–V–M (M = Si, Nb, Ta) ternary systems, Intermetallics 118 (2020) 106701, https://doi.org/10.1016/j.intermet.2020.106701.
[84] T. Doi, H. Ishida, T. Umezawa, Study of Nb-Zr-Ti phase diagram (studies of hard superconductor, II), J. Jpn. Inst. Metals 30 (1966) 139–145, https://doi.org/10.2320/jinstmet1952.30.2_139.
[85] L. Lin, L. Delaey, O. Van Der Biest, P. Wollants, Calculation of isothermal sections of three ternary Ti-Zr-X systems, Scr. Mater. 34 (1996) 1411–1416, https://doi.org/10.1016/1359-6462(96)00006-1.
[86] T. Tokunaga, S. Matsumoto, H. Ohtani, M. Hasebe, Thermodynamic calculation of phase equilibria in the Nb-Ni-Ti-Zr quaternary system, Mater. Trans. 48 (2007) 89–96, https://doi.org/10.2320/matertrans.48.89.
[87] C. Marker, S. Shang, J. Zhao, Z. Liu, Thermodynamic description of the Ti-Mo-Nb-Ta-Zr system and its implications for phase stability of Ti bio-implant materials, Calphad 61 (2018) 72–84, https://doi.org/10.1016/j.calphad.2018.02.004.
[88] P.E.J. Flewitt, A re-assessment of the monotectoid loop (β-Nb+β-Zr) in the niobium–zirconium system, J. Appl. Crystallogr. 5 (1972) 423–425, https://doi.org/10.1107/S0021889872010076.
[89] K. Korniyenko, in: Niobium-Vanadium-Zirconium, 2010, pp. 533–542, https://doi.org/10.1007/978-3-642-00771-2_44.
[90] I.I. Gorbachev, V. V Popov, A. Katz-Demyanetz, V. Popov, E. Eshed, Prediction of the phase composition of high-entropy ?lloys based on Cr–Nb–Ti–V–Zr using the Calphad method, Phys. Met. Metallogr. 120 (2019) 378–386, https://doi.org/10.1134/S0031918X19040069.
[91] M. Enomoto, The Ti-V-Zr system (titanium-vanadium-zirconium), J. Phase Equil. 13 (1992) 206–210, https://doi.org/10.1007/BF02667490.
[92] A. Nowikow, H.G. Baer, Das dreistoffsystem titan-vanadin-zirkon, Int. J. Mater. Res. 49 (1958) 195–199, https://doi.org/10.1515/ijmr-1958-490406.
[93] G.B. Bokas, W. Chen, A. Hilhorst, P.J. Jacques, S. Gorsse, G. Hautier, Unveiling the thermodynamic driving forces for high entropy alloys formation through big data ab initio analysis, Scr. Mater. 202 (2021) 114000, https://doi.org/10.1016/j.scriptamat.2021.114000.
[94] D. de Fontaine, The number of independent pair-correlation functions in multicomponent systems, J. Appl. Crystallogr. 4 (1971) 15–19, https://doi.org/10.1107/S0021889871006174.
[95] A.V. Ceguerra, R.C. Powles, M.P. Moody, S.P. Ringer, Quantitative description of atomic architecture in solid solutions: a generalized theory for multicomponent

short-range order, Phys. Rev. B Condens. Matter (2010), https://doi.org/10.1103/PhysRevB.82.132201.
[96] J.M. Goff, B.Y. Li, S.B. Sinnott, I. Dabo, Quantifying multipoint ordering in alloys, Phys. Rev. B 104 (2021) 054109, https://doi.org/10.1103/PhysRevB.104.054109.
[97] S. Dasari, A. Sharma, C. Jiang, B. Gwalani, W.-C. Lin, K.-C. Lo, S. Gorsse, A.-C. Yeh, S.G. Srinivasan, R. Banerjee, Exceptional enhancement of mechanical properties in high-entropy alloys via thermodynamically guided local chemical ordering, Proc. Natl. Acad. Sci. USA 120 (2023), https://doi.org/10.1073/pnas.2211787120.